

THESIS

VARIATION IN CHROMOSOMAL ABERRATION INDUCTION IN DIFFERING ATM
AND ASPM GENOTYPIC BACKGROUNDS DETECTED VIA A MODIFIED PNA FISH
TECHNIQUE

Submitted by

Ashley Romero

Department of Environmental and Radiological Health Sciences

In partial fulfillment of the requirements

For the Degree of Master of Science

Colorado State University

Fort Collins, Colorado

Summer 2013

Master's Committee:

Advisor: Takamitsu Kato

Joel Bedford
Douglas Thamm

Copyright by Ashley Romero 2013

All Rights Reserved

ABSTRACT

VARIATION IN CHROMOSOMAL ABERRATION INDUCTION IN DIFFERING *ATM* AND *ASPM* GENOTYPIC BACKGROUNDS DETECTED VIA A MODIFIED PNA FISH TECHNIQUE

A modified PNA (peptide nucleic acid) FISH (fluorescence *in situ* hybridization) method has been developed for efficient quantitative and qualitative analysis of chromosomal aberration formation. PNA FISH was used to detect a heightened sensitivity in mouse fibroblasts in response to ionizing radiation with *Atm*^{-/-} and in mouse embryonic fibroblasts (MEFs) in response to loss of the *Aspm* gene respectively. For *Atm* analysis, four commonly used inbred mouse strains were used, C57BL/6J, A/J, 129S6, and BALB/cByJ, and exposed to cesium-137 at a dose rate of approximately 2.5 Gy/min. For *Aspm* analysis, MEF cell lines were used and exposed to 0.2 μM tamoxifen for inducible Cre-lox excision of floxed *Aspm* alleles. Upon analysis of chromosome-type aberrations, there were statistically significant elevations in acentric fragment and/or dicentric average frequencies seen across all strain backgrounds of the *Atm*^{-/-} genotype, however, only the 129S6 *Atm*^{-/-} strain backgrounds exhibited a significant increase in mean telomere-associated fusion events. In addition, there was a heightened dose response from a 0 to 2 Gy dose in *Atm*^{-/-} BALB/cByJ and C57BL/6J backgrounds indicating a lack of synergism of the Prkdc (protein kinase, DNA-activated, catalytic polypeptide) defect in BALB/cByJ strains. For *Aspm* analysis, in comparison to control, or untreated, MEF strains, there was an increased average aberration frequency in *Aspm*^{-/-} cell lines over a 48-hour time period. However, there was also an increased frequency in *Aspm*^{+/-} cell lines comparable to the frequency observed in *Aspm*^{-/-} cells, which is characteristic of haploinsufficiency. Therefore, not only is *Atm* status an important determinant of radiosensitivity, but strain backgrounds can also contribute to a heightened

response. In addition, *Aspm* expression is critical for the maintenance and repair of DNA. Together, this data suggests that the *Atm* and *Aspm* genes are crucial components in the preservation of chromosomal integrity and genomic stability in response to DNA damage.

ACKNOWLEDGEMENTS

I would like to acknowledge and thank the National Institute of Radiological Sciences for the use of their facilities and the opportunity of collaborating with them in this research as well as the opportunity to be apart of the open laboratory experience. I would also like to especially thank Dr. Fujimori for providing the MEF cell strains used in the *Aspm* project and the support of his expertise.

I would also like to express my appreciation to the Environmental and Radiological Health Sciences Department at Colorado State University for all help with regards to this project in using their equipment and laboratory. I would especially like to thank Dr. Weil, Dr. Genik, and Dr. Nagasawa for their knowledge, for characterizing and supplying the mice strains, and for preparation of the primary cell cultures used in the *Atm* project.

I would especially like to thank and express my appreciation to my advisor and mentor Dr. Takamitsu Kato who has provided me with a multitude of educational experiences as well as for his encouragement and direction. It has been a privilege to work in his lab and to learn the many laboratory techniques that helped me grow as a graduate student. I would also like to thank my committee members Dr. Joel Bedford and Dr. Douglas Thamm for their support, guidance and expertise.

I am very grateful and appreciative of the support and assistance provided by my fellow laboratory colleagues Ian Cartwright, Justin Bell, and Carissa Burke who selflessly donated their time and efforts in completing this project.

TABLE OF CONTENTS

ABSTRACT.....	ii
ACKNOWLEDGEMENTS.....	iv
TABLE OF CONTENTS.....	v
LIST OF TABLES.....	vii
LIST OF FIGURES.....	viii
LIST OF SYMBOLS.....	ix
LIST OF ACRONYMS.....	x
CHAPTER ONE - INTRODUCTION	
1.1. GENOMIC INSTABILITY AND DNA DAMAGE.....	1
1.1.1. Chromosomal aberrations.....	2
1.1.2. DNA repair pathways.....	5
1.2. <i>ATM</i> AND <i>ASPM</i>	7
1.2.1. <i>ATM</i> and DNA repair.....	11
1.2.2. <i>ATM</i> disruption.....	11
1.2.3. <i>ASPM</i> function.....	12
1.2.4. <i>ASPM</i> disruption.....	13
1.3. CYTOGENETIC ASSAYS.....	14
1.3.1. Advancements in cytochemical techniques.....	15
1.3.2. PNA FISH.....	15
CHAPTER TWO – Strain Dependent Variations in Radiation-Induced Chromosome-type Aberrations on <i>Atm</i>^{+/+} and <i>Atm</i>^{-/-} Genotypic Backgrounds.	
2.1. BACKGROUND.....	19
2.2. MATERIALS AND METHODS.....	20
2.2.1. Cell culture.....	21

2.2.2. Irradiation.....	22
2.2.3. Metaphase chromosome preparation	22
2.2.4. Modified PNA FISH method	23
2.2.5. Scoring method for chromosome aberrations	23
2.2.6. Statistical Analysis.....	23
2.3. RESULTS	24
2.4. DISCUSSION	29
CHAPTER THREE - Induction of Chromosomal Aberrations Consequent to <i>Aspm</i>	
Excision Via the Cre-Lox Recombination System.	
3.1. BACKGROUND	30
3.2. MATERIALS AND METHODS.....	31
3.2.1. Cell culture.....	34
3.2.2. Metaphase chromosome preparation	35
3.2.3. Modified PNA FISH method	35
3.2.4. Scoring method for chromosome aberrations.....	36
3.2.5. Statistical analysis.....	36
3.3. RESULTS	36
3.4. DISCUSSION.....	40
CHAPTER FOUR – CONCLUSIONS	41
REFERENCES.....	43
APPENDIX I	50

LIST OF TABLES

Table 1: Origin and <i>Atm</i> status of mouse cells.....	21
Table 2: Summary of aberration frequencies for C57BL/6J, BALB/cByJ, A/J and 129S6 <i>Atm</i> ^{+/+} and <i>Atm</i> ^{-/-} strain backgrounds	25
Table 3: Origin and <i>Aspm</i> status of mouse cells	34
Table 4: Summary of aberration frequencies for MEF strains across differing <i>Aspm</i> genotypes	37
Table 5: Signal strength over time	52
Table 6: Signal strength over varying temperatures	53

LIST OF FIGURES

Figure 1: Examples of chromosome-type aberrations in metaphase murine chromosome spreads as detected by DAPI staining and PNA hybridization.....	4
Figure 2: Representation of the NHEJ DNA repair pathway	6
Figure 3: Schematic representation of the <i>ATM</i> gene.....	8
Figure 4: Molecular location of the <i>ASPM</i> gene.....	10
Figure 5: Comparison of PNA FISH and Giemsa staining techniques.....	18
Figure 6: Comparison of average dicentric aberration yield over a 0, 1, and 2 Gy dose for each strain background of <i>Atm</i> ^{+/+} and <i>Atm</i> ^{-/-} genotypes.....	26
Figure 7: Comparison of average acentric fragment yield over a 0, 1, and 2 Gy dose for each strain background of <i>Atm</i> ^{+/+} and <i>Atm</i> ^{-/-} genotypes.	27
Figure 8: Comparison of average telomere-associated fusion yield over a 0, 1, and 2 Gy dose for each strain background of <i>Atm</i> ^{+/+} and <i>Atm</i> ^{-/-} genotypes.....	28
Figure 9: The loxP sequence.....	32
Figure 10: Diagram representing variations of the Cre-lox recombination system.....	33
Figure 11: Average dicentric frequencies compared at 0 (Control), 24-hour, and 48-hour time points.....	38
Figure 12: Average acentric fragment formation frequency across 0 (Control), 24, and 48-hour time period.....	39

LIST OF SYMBOLS

°C	degrees Celsius
%	percentage
bp	base pairs
Gy	Gray
Gy/min	Gray per minute
kb	kilobases
kDa	kilo Daltons
µg/ml	micrograms per milliliter
µl	microliter
µm	micrometer
mg/ml	milligram per milliliter
ml	milliliter
min	minute
mM	millimolar
M	molar
nM	nanomolar
U/ml	units per milliliter

LIST OF ACRONYMS

ANOVA	analysis of variance
ASPM	abnormal spindle-like microcephaly-associated
ATM	ataxia telangiectasia mutated
BER	base excision repair
BrdUrd	5`-bromodeoxyuridine
CO ₂	carbon dioxide
DAPI	4`, 6-diamidino-2-phenylindole
DNA	deoxyribose nucleic acid
DNA-PK	DNA-dependent protein kinase
DNA-PKcs	catalytic subunit of the DNA-dependent protein kinase
DSB	double-strand break
ER	estrogen receptor
FBS	fetal bovine serum
FEN1	flap endonuclease 1
FISH	fluorescence <i>in situ</i> hybridization
FRAP	FKBP12 rapamycin-associated protein
HCl	hydrogen chloride
HiCEP	high-coverage expression profiling
HR	homologous recombination
IQ	isoleucine-glutamine
IR	ionizing radiation
KCl	potassium chloride
MCPH	autosomal recessive primary microcephaly
MEF	mouse embryonic fibroblasts

MEM	minimal essential medium
MMR	mismatch repair
mRNA	messenger RNA
NE	neuroepithelial
NER	nucleotide excision repair
NHEJ	non-homologous end-joining
PBS	phosphate-buffered saline
PCC	premature chromosome condensation
PCR	polymerase chain reaction
PFA	paraformaldehyde
PNA	peptide nucleic acid
PRKDC	protein kinase, DNA-activated, catalytic polypeptide
RNAi	RNA interference
siRNA	small interfering RNA
SSB	single-strand break
TRRAP	transformation/transcription domain-associated protein

CHAPTER ONE

INTRODUCTION

1.1. GENOMIC INSTABILITY AND DNA DAMAGE

Genomic instability is a condition where the rate of introduction of genomic changes is elevated relative to the normal condition (1). The genomic changes can be attributed to genetic alterations and environmental influences resulting in cellular damage including gene mutation, gene amplification, chromosomal destabilization, and cellular transformation (2). The direct or indirect damages that accumulate from transient or prolonged exposures to DNA damaging agents are presumably the impetus needed for carcinogenicity. Exposure to ionizing radiation, e.g. X-rays or gamma rays, exemplifies a catalyst for genomic alterations manifested through chromosomal destabilization and rearrangements. DNA single-strand breaks (SSBs) and DNA double-strand breaks (DSBs) are such lesions that occur with exposure to clastogenic agents, such as ionizing radiation, but also are a result of natural biological processes such as replication and recombination events in the cell cycle (3). DNA SSBs, lesions that occur on one strand of the chromosome, after exposure to ionizing radiation are able to efficiently be repaired in normal cells, however, DNA DSBs, lesions that occur on both strands of the chromosome, can have genotoxic results due to incomplete restoration of the DNA. Due to the more critical outcomes that are associated with DNA DSBs, including radiation-induced chromosomal damage, mutagenesis, and cell killing, it has become an increasingly important topic to study in order to elucidate underlying molecular mechanisms of disease onset and progression (4-6). Cytogenetic assays of radiation-induced cellular changes have become a more important focus in radiobiological studies over the years in the wake of innovative genetic research. Such research includes studies done with *Drosophila* where spontaneous mutations were comparable to the mutations induced by X-ray treatment. However, by observation of *Drosophila* sperm cells and oocytes, the

transforming action of X-rays caused other genetic problems other than gene mutations. It was found that the condition of the chromosomes themselves were being compromised which was reflected in altered rearrangement, fragmentations, and inversions of portions of the chromosomes (7). A closer look at causation takes us further into the microcosm of the nucleus of the cell, the chromosomes that are housed within and the diverse lesions that can arise.

1.1.1. Chromosomal aberrations

In order to observe the lesions in their entirety, cells are examined at the first metaphase after exposure to ionizing radiation or a radiomimetic drug. The structural alterations that can be distinguished upon observation of the chromosomes can be categorized into chromosome- or chromatid-type aberrations (8). Chromosome-type aberrations arise when the damage to an unduplicated chromatid thread, corresponding to the pre-DNA synthesis stage of the cell cycle, is passed along to the duplicated chromosome. Chromatid-type aberrations occur when damage is inflicted to only one of the sister chromatids after duplication at the time of exposure (8). However, for the purposes of this thesis, only chromosome-type aberrations will be discussed. Two primary structures that are involved in improper or incomplete biological processes that result in chromosome-type aberrations are the centromere and telomere structures. The centromere, or kinetochore, is the primary constriction point between two sister chromatids and it is at these foci during anaphase of the cell division cycle where spindle organization occurs for migration of the chromosomal piece to opposite poles of the cell (9, 10). Telomeres are nucleoprotein structures consisting of repetitive sequences of (TTAGGG)_n that cap the ends of eukaryotic chromosomes and play important roles in preservation of genomic stability through end protection and maintenance of chromosomal ends (11). Radiation-induced cellular damage resulting in commonly observed chromosome-type lesions involving these structures are classified as exchange-type

aberrations, or aberrations resulting from illegitimate reunions involving two or more double-strand breaks. An example of this aberration is known as a dicentric where one of the two interchanged chromosomes now have two centromeres (12). Within the occurrence of a dicentric, further classification is applied to account for telomere abnormalities which occur when cellular damage or improper telomere regulation and maintenance results in the recognition of DNA ends as double-strand breaks consequently activating cell cycle checkpoint responses and aberrant recombination events resulting in fusions (11, 13, 14). Figure 1 highlights examples of these chromosome-type aberrations through PNA FISH.

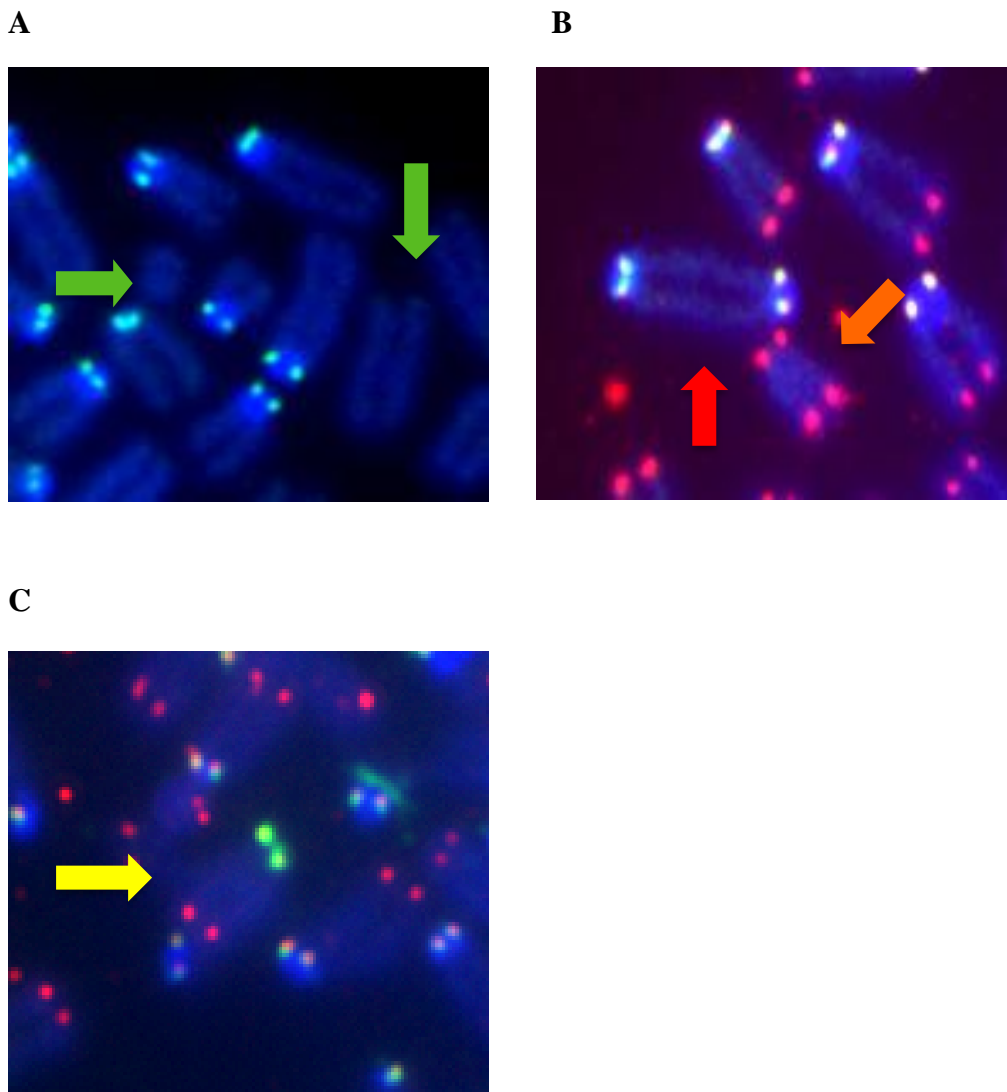


Figure 1. Examples of chromosome-type aberrations in metaphase murine chromosome spreads as detected by DAPI (diamidino-2-phenylindole) staining and PNA hybridization. (A) Acentric fragments designated at both green arrows. (B) A complete asymmetrical interchange (top red arrow) accompanied by an acentric fragment, or compound fragment (bottom orange arrow). (C) A telomere-associated fusion event (yellow arrow).

1.1.2. DNA repair pathways

Cellular compensation mechanisms that are specific for DNA SSBs and DNA DSBs include mismatch repair (MMR), base excision repair (BER), nucleotide excision repair (NER), non-homologous end-joining (NHEJ), and homologous recombination (HR) (15). The repair mechanisms that are specific to DNA DSBs are NHEJ and HR. The non-homologous end-joining (NHEJ) DNA pathway is the primary repair mechanism for DSB repair in the initial G₀/G₁ phases of the cell cycle in response to ionizing radiation and is relatively independent of terminal DNA sequence homology when joining the two ends of a DSB and produces junctions that vary in sequence composition as shown in Figure 2 (16, 17).

Non Homologous End Joining

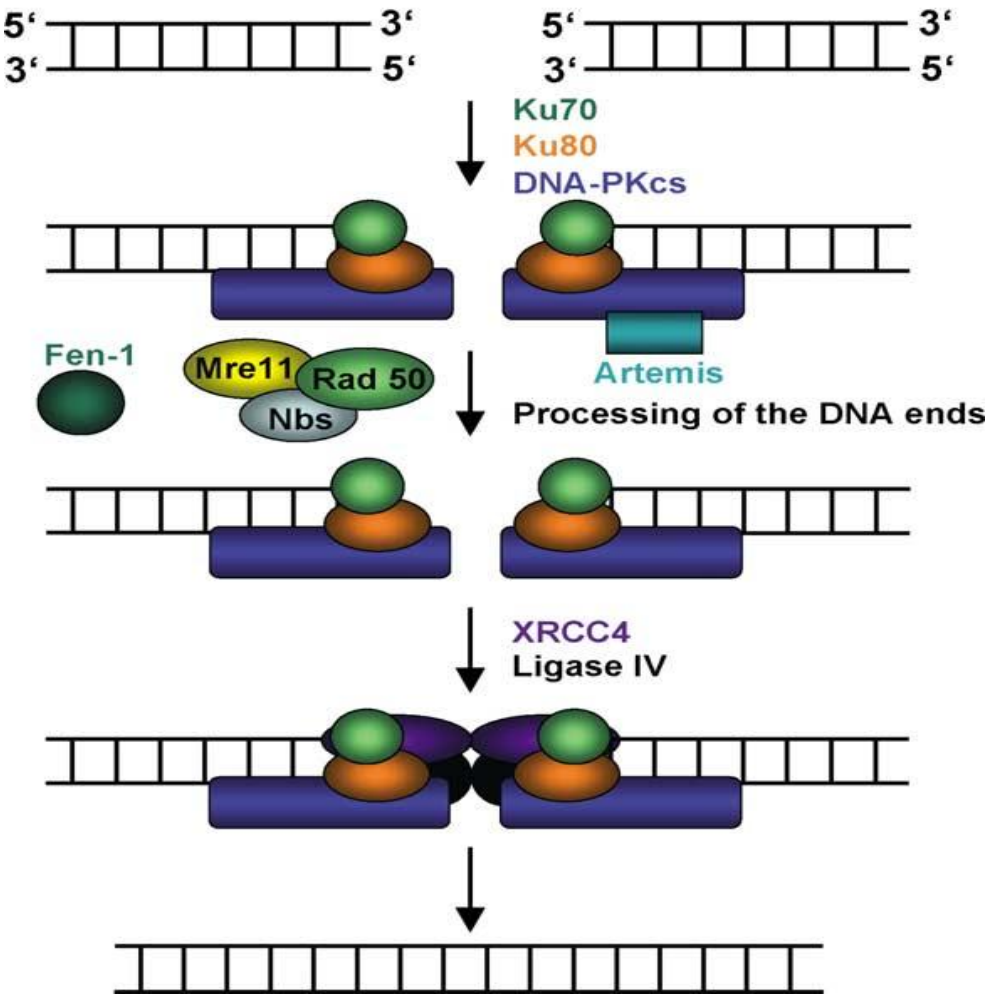
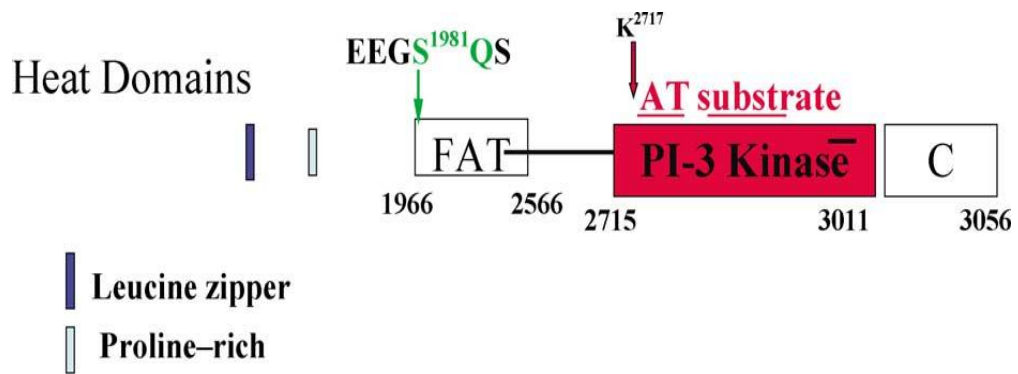


Figure 2. Representation of the NHEJ DNA repair pathway (15).

Specifically, the Ku heterodimer, Ku80/Ku70, binds to the end of the DNA fragments and activates the catalytic subunit of DNA-PK (DNA-dependent protein kinase) which interacts with other cofactors, such as XRCC4 and Ligase IV, to provide a linkage between the two DNA strands. Processing of the 5' and 3' overhangs is done through a protein kinase, ataxia telangiectasia mutated (ATM), the MRN complex comprised of MRE11, RAD50, and NBS1, and presumably the flap endonuclease 1 (FEN1) (15). Dysfunction of one or more of these proteins can lead to diseased states resulting in hypersensitivity to various DNA-damaging agents where long-term exposure increases susceptibility to the development of cancer.

1.2. *ATM* AND *ASPM*

Two such important genes associated with DNA repair, that when compromised can lead to debilitating susceptibilities, are *ATM* and *ASPM*. The ATM, ataxia telangiectasia mutated, protein has sequence homology to the phosphatidylinositol-3-OH-kinase family of proteins and is a relatively large protein extending over 160 kb of genomic DNA containing 66 exons giving rise to a 350 kDa protein (18, 19). The kinase activity of the protein occurs at the C-terminal end where the FAT (FRAP, ATM, TRRAP)- related, domain maintains influence on the adjacent kinase domain and its activity as seen in Figure 3 (20).



Optimal Substrates:

G-L/F/M-A-Q/F/M-M/F-Q/P-L-S-Q-E/Q-V/Q/P-F-A

Figure 3. Schematic representation of the *ATM* gene. (19).

The *ASPM*, abnormal spindle-like microcephaly-associated protein, gene encoding a 10,434 bp coding sequence with 28 exons spanning 65 kb of genomic DNA is mapped on chromosome 1q31 as depicted in Figure 4. The gene consists of four regions: the microtubule-binding N-terminal domain, a calponin-homology domain, isoleucine-glutamine (IQ) repeat domain, and a C-terminal region (21, 22). The expression of each gene is essential for maintaining chromosomal integrity, therefore, each play an important role in the preservation of genomic stability.

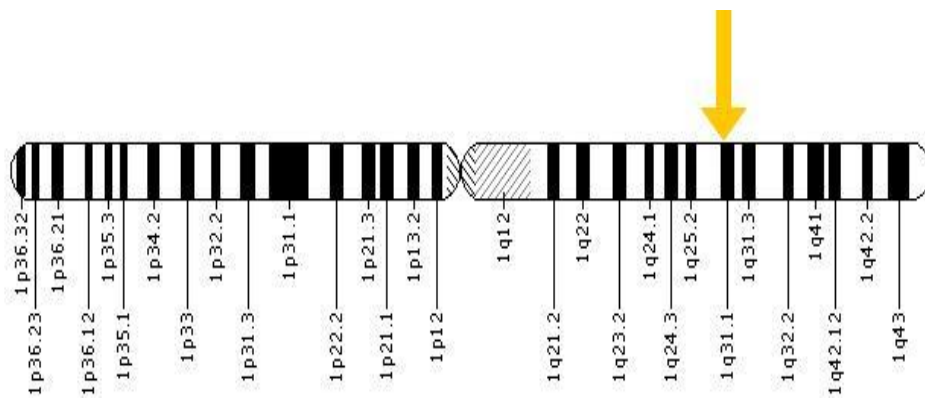


Figure 4. Genetic map of the *ASPM* gene. The *ASPM* gene is mapped on the long (q) arm of chromosome 1 at position 31 (23).

1.2.1. ATM and DNA repair

Primarily, the ATM protein is one of the primary responders to DNA DSBs by increasing its kinase activity for preparation of a series of phosphorylation events, specifically, targeting threonine and serine residues followed by glutamine (SQ/TQ motifs). Prior to activation, ATM is held in an inactive dimeric or multimeric form where the kinase domain is blocked by the FAT region of the other. When DNA damage occurs, autophosphorylation at Ser1981 residues will allow the proteins to transform into active monomeric forms where after damage is inflicted, ATM is recruited to the DSB sites where enzymatic reactions such as signaling transduction through phosphorylation of various downstream substrates such as the MRN complex, checkpoint proteins, γ -H2AX, among others (24).

1.2.2. ATM disruption

Mutations can occur throughout the gene, most of which are truncating or missense, and consequently can result in the decreased production of the protein, or a reduction in kinase activity with normal amounts of the protein produced (19). Therefore, if *ATM* is compromised and in response to ionizing radiation, the rejoining capacity of the cell is hindered leading to an increase in chromosomal damage and a decrease in cellular viability. The cell's progeny is also affected due to continued proliferation despite any damage incurred due to the lack of G₁/S phase checkpoint activation to allow for cellular arrest and proper ATM-dependent repair (25). Consequent to mutations of the *ATM* gene, debilitating effects ensue such as a condition characterized by hypersensitivity to radiation, cancer susceptibility, immune dysfunction, and decreased neurological function. Ataxia telangiectasia (A-T) is a rare, early onset neurological disorder characterized by hypersensitivity to ionizing radiation, immunodeficiency, cancer susceptibility, and motor deficits. Young children, usually between 2-3 years of age, begin expressing the classical A-

T phenotype initially with ataxia, which renders them incapable to walk by age ten. Oculocutaneous telangiectasias, dilated blood vessels, appear usually after the onset of neurological symptoms such as oculomotor apraxia and dysarthria. Most patients are immunodeficient with frequent sinopulmonary infections and predisposed to cancer, usually lymphoid (26). The disease is autosomal recessive with cells exhibiting null mutation in both copies of the *ATM* gene, however, individuals exhibiting heterozygosity have shown to have an increase in cancer predisposition, albeit a less severe phenotype, depending on the nature of the mutation in which a dominant negative effect can further disrupt ATM signaling (18, 26). A demonstrable model in this disease progression can be found in mice due to an 84% amino acid identity and 91% similarity to the *ATM* homolog (27). Mice that are rendered nullizygous via disruption of *Atm* through gene targeting exhibit a similar phenotype to that of individuals with A-T in which growth retardation, neurologic dysfunction, sterility, and thymic lymphoma formation was observed (28).

1.2.3. *ASPM* function

Interspecies comparisons of *ASPM* homologues reveal that a larger brain size is correlated with a greater number of IQ repeats and thus a larger protein size (22). In addition, it has been suggested that the evolving *ASPM* gene may have been positively selected in hominids due to highly conserved coding and noncoding regions (21). The *ASPM* gene is a homologue to the *asp* (abnormal spindle) gene of *Drosophila melanogaster* where it is known to be essential for the organization of structural components, microtubule and mitotic spindle development, during mitosis and meiosis (29). This can be attributed to the resultant gene product that is reported to be a spindle pole/centrosome protein (30). This aspect was also studied in mouse embryonic neuroepithelial (NE) cells where the loss of *Aspm*, via RNA interference (RNAi), resulted in centromere detachment from sister chromatids, and thus altering spindle position during mitosis. Consequently, an alteration of the cleavage plane

increased the probability of asymmetrical division (31). The *ASPM* gene is preferentially expressed in embryonic and fetal mammalian neuroepithelium, however, in human adults, *ASPM* mRNA is also expressed in the breast, lung, pancreas, uterus, colon, thyroid, liver, bladder, kidney, ovary, testis, stomach, lymph node, cervix, and esophagus, but expression was not found in the brain and skeletal muscle (22, 32-34).

1.2.4. *ASPM* disruption

Because the *ASPM* gene is responsible for proper cell division, mutations result in the mitotic arrest of neuroblasts resulting in an underdeveloped central nervous system (33, 35, 36). In humans, cerebral cortical size is diminished in individuals that carry the mutated gene. Specifically, mutations at the MCPH₅ locus of the *ASPM* gene causes a rare condition called autosomal recessive primary microcephaly (MCPH) which is characterized by a reduction in fetal brain growth and thus a reduction in head circumference, particularly the cerebral cortex (37). As a result, a small but structurally normal brain size and accompanied mental retardation occurs, but no other neurological abnormalities are observed (22, 38). These outcomes have also been induced through ionizing radiation as seen in atomic bomb survivors of Hiroshima and Nagasaki as well as artificial induction by exposing laboratory mice in utero. The mouse homologue, *Aspm*, exhibits 74.4% homology to the human *ASPM* gene and therefore is an adequate model for studying functionality and disease mechanisms. Similar mutational outcomes are seen in the brain of *Mus musculus* where the *Aspm* gene plays a central role in cerebral cortical neurogenesis (22). To underline this role in neurogenesis, Pulvers et. al. created two mutant mouse cell lines, *Aspm*^{L-25} and *Aspm*^{L-7}, containing truncating mutations in the microtubule-binding domain and C-terminal amino acids respectively to mimic the phenotype expressed by human microcephaly patients. Indeed there was a decrease in brain size and weight in both mutated mice, however, the severity of the outcome was less than that seen in human primary microcephaly (39). Aside

from mutant alterations, it has been suggested, through studies with fetal murine neural cells, that the mechanism underlying microcephaly was through cell killing through ionizing radiation exposure which reduces the number of neural stem/progenitors during cellular proliferation at day 11-14 fetal brains (40, 41). In addition, Fujimori et al. proposed another mechanism suggesting that through radiation-induced downregulation of the *Aspm* gene, symmetric division of neuronal progenitors is suppressed resulting in a reduction of neuronal cells and thus microcephaly (42).

1.3. CYTOGENETIC ASSAYS

In order to elucidate mechanisms of disease initiation and progression resulting from genetic disruption, chromosomal alterations must be examined and so cytogenetic assay have become an integral tool for analysis at the level of the individual cell (43). A variety of cytogenetic assays have been developed for the independent or simultaneous genotoxicological monitoring of chemical agents, pharmaceuticals, and mutagens. For example, the chromosome aberration analysis assay is used to detect chromosomal anomalies in metaphase spreads where structural and/or numerical aberrations are scored. Another technique is the micronucleus cytokinesis-block assay which takes advantage of cells that express micronuclei through the identification of their binucleate appearance through the inhibition of cytokinesis by cytochalasin-B (44). Sister-chromatid exchanges are measured and visualized through the incorporation of a DNA base analog 5'-bromodeoxyuridine (BrdUrd) for the standard fluorescence and Giemsa staining method or alternatively, the utilization of antibody detection (45). The premature chromosome condensation (PCC) method involves the fusion of mitotic with interphase cells and provides a way to analyze the fragility of chromatin, or capacity to repair initial damage from radiation exposure (46, 47). In conjunction with molecular identifiers, qualitative analysis is enhanced by

strengthening the resolution of these assays, thereby ensuring consistent, quantifiable data for the generation of dose-response relationships.

1.3.1. Advancements in cytochemical techniques

Over the years, the development of cytochemical techniques for the identification and detection of cellular structures has led to improved methods that allow a more specific and detailed view at the molecular level. Historically, non-specific natural and synthetic dyes were used to label general molecular entities such as basic proteins, nucleic acids, and carbohydrates. In the early 1940`s, fluorescently conjugated antibodies were developed which led to the first antibody-dependent fluorescent detection of nucleic acid hybrids (48, 49). In the late 1960`s, the earliest in situ hybridization utilizing radiolabeled probes consisting of non-specific labeling through the random incorporation of radioactive modified bases into growing cells and autoradiography (48, 50). Finally, in 1980, the first application of fluorescent in situ detection was developed where fluorophore-labeled RNA was used as a probe for DNA sequences (51). In the years following, improved hybridization methods for direct labeling of synthetic, single-stranded DNA probes were created for better sensitivity and resolution for fluorescent detection (52). For example, multicolor banding (mBAND) is a painting technique which is used to detect any aberration leading to the loss or rearrangement of longitudinal colored bands along the axis of the chromosome (53). Another painting technique used for the detection of intrachanges, among other aberrations, is the PNA FISH technique.

1.3.2. PNA FISH

A specific and sophisticated qualitative cytogenetic technique used to measure the effects of cellular damage is the PNA (peptide nucleic acid) FISH (fluorescence *in situ* hybridization) method. This method was developed for studies involving chromosome structure and function, genome mapping, and clinical cytogenetics and has become more

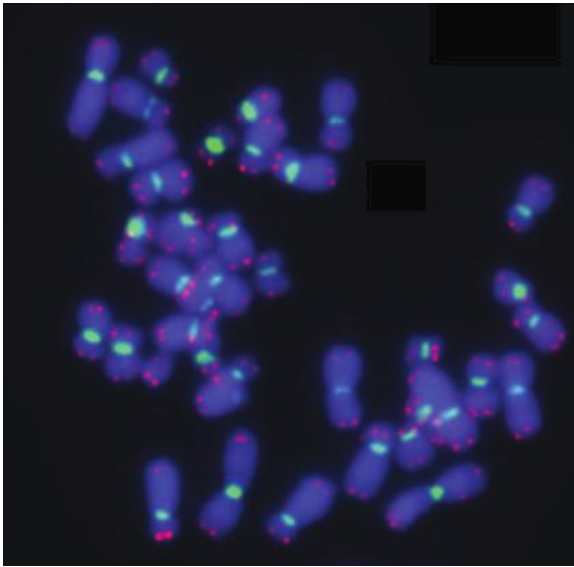
widely used due to its high hybridization efficiency and its high reproducibility (54, 55).

Fluorescent *in situ* hybridization (FISH) is a technique using molecular DNA probes for the detection of complementary DNA sequences along a chromosome. Peptide nucleic acids (PNAs) mimic nucleic acids such that they contain pseudo-peptide backbone that consist of charge neutral and achiral N-(2-aminoethyl) glycine units where the nucleobases are connected through a methylene carbonyl linker (56-58). The fluorochrome-labeled PNA oligomers then hybridize to tandem DNA repeats such as telomeres (TTAGGG) and centromeres with high affinity and specificity. Together with the application of the DAPI counterstain, the signals can then be clearly seen with fluorescent microscopy and the proper imaging software. Traditionally, for the probe to hybridize to DNA, both have to be rendered single-stranded through the application of heat in a formamide solution followed by hybridization of the probe which requires multiple hours (59). However, the modified method used for these experiments does not require denaturation and ranges in hybridization periods from 6 to 18 hours (Appendix 1). Visually, this method provides a clear distinction between simple and complex chromosomal aberrations that arise from radiation-induced damage in cytological preparations. This technique provides a more in depth look into the various types of telomeric and centromeric chromosomal aberrations such as dicentric formation and telomeric fusions that cannot be seen with other practical staining methods such as the Giemsa stain. Although, the Giemsa stain will allow for the identification of exchanges and other chromosomal structural rearrangements, this stain does not account for other structural entities that may provide a more mechanistic view of damage induction (Figure 5).

Specifically, the modified PNA FISH technique was utilized to examine our overall hypothesis through the detection and identification of chromosome aberrations due to an increased cellular sensitivity in response to radiation exposure and/or genotypic variation of two genes involved in DNA repair, *Atm* and *Aspm*. This methodology allowed for the

characterization of three different types of chromosome-type aberrations that may be indistinguishable through other conventional cytogenetic techniques.

A



B

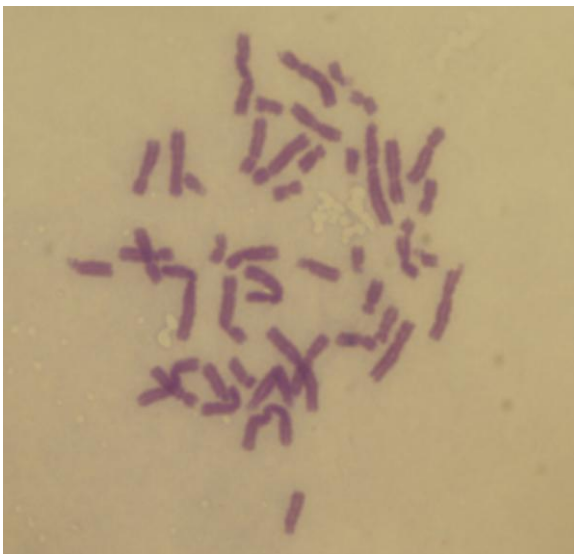


Figure 5. Comparison of PNA FISH and Giemsa staining techniques. (A) FISH-labeled human peripheral lymphocyte chromosome spread. (B) Human fibroblast chromosome spread shown with Giemsa stain. With PNA FISH centromere and telomere structures are clearly identifiable and distinguished through the use of the probe specificity against a DAPI background.

CHAPTER TWO

Strain Dependent Variations in Radiation-Induced Chromosome-type Aberrations on *Atm*^{+/+} and *Atm*^{-/-} Genotypic Backgrounds.

2.1. BACKGROUND

Differences in radiosensitivity in response to a particular dose of radiation have proven to be dependent upon the capacity of the cell to repair DNA DSBs which can lead to differences in cell killing sensitivity, chromosome aberrations production, or mutation induction (60). A previous study has shown that cells from *Atm*^{-/-} mice showed an increase in radiosensitivity as detected by an increase in γ -H2AX mean foci formation per cell via the γ -H2AX assay in comparison to *Atm*^{+/+} and *Atm*^{+/-} cell strains in response to acute high-dose radiation exposure. This same γ -H2AX assay was used to distinguish a 2.7-fold increase in average foci per cell in response to low dose-rate radiation exposure between *Atm*^{+/+} and *Atm*^{+/-} cells and a 6.3-fold larger increase for *Atm*^{-/-} cells. The implications of these results indicate the occurrence of mild hypersensitivities in even heterozygous populations in response to radiation exposure and the initial mechanism of disease progression is predicated on DNA DSB processing and repair (61). However, experimental outcomes with mice of differing genetic backgrounds for the *Atm* gene in conjunction with differing mice strains are not well known. Therefore, we used four different inbred mice strains, C57BL/6J, BALB/cByJ, A/J, and 129S6, to quantify variations in genetic background, *Atm*^{+/+} and *Atm*^{-/-}, resulting in a uniformly increased radiosensitivity that might increase or reduce to the sensitivity of the mice on these different backgrounds. The BALB/cByJ strain carries a hypomorphic allele of a protein kinase, DNA-activated, catalytic polypeptide (Prkdc or DNA-PKcs), a key component of the NHEJ pathway in repairing radiation-induced double-strand breaks, and so mice of this background would be expected to be especially sensitive to neoplastic formation and genomic instability (62). The C57BL/6J mice are a commonly used

inbred strain that provides a controlled background in mutation expression due to its resistance to most tumor formations. These mice are often used as an experimental control as is the 129S6 strain, due to relatively normal fecundity and viability. The A/J strain is another widely used strain for cancer research and has a high incidence of spontaneous lung tumors and myoepitheliomas (63, 64). However, not much is known about the radiosensitivity of these strains in conjunction with the differing *Atm* backgrounds. Given the various mutations that can occur throughout the gene as well as the relatively large size of it, it is difficult and expensive to isolate and study. Therefore, we hypothesized a variation in radiosensitivity across the four inbred strains and that a *Atm*^{-/-} genotypic background results in an increased radiosensitivity that adds to or reduces the sensitivity of the mice strains. Radiosensitivity was detected through the formation of chromosomal aberrations via a modified PNA FISH technique.

2.2. MATERIALS AND METHODS

The cell strains were primary cultures derived from ear punch biopsies from adult mice that were being used to generate congenic strains for the *Atmtm1Awb* knockout allele. The founder strain is 129S6/SvEvTac-*Atmtm1Awb*. At the time tissues were collected, the knockout allele was fully introgressed onto an A/J background and partially introgressed onto the CBA/J background. The progeny of *Atmtm1Awb*/1 × *Atmtm1Awb*/1 matings were genotyped by PCR amplification of tail snip DNA using a protocol provided by Dr. Carolee Barlow (65). The amplification primers used were GACTTCTGTCAGATGTTGCTGCC (ATM-F), CGAATTTGCAGGAGTTGCTGAG (ATM-B), and GGGTGGGATTAGATAAATGCCTG (ATM-Neo). Mating and genotyping were performed under protocol no. 03-132A of the Colorado State University Animal Care and Use Committee and were funded by the Ataxia-Telangiectasia Children's Project. BALB/cByJ *Atmtm1Awb* congenic mice were generated by thirteen generations of conventional

backcrosses followed by five intercross generations. These congenic strains are available from the Jackson Laboratory (Bar Harbor, ME). *Atm*^{-/-} mice are infertile so the congenic strains are maintained with *Atm*^{+/-} breeders (66). The strains, genotypes and sex of mice used for establishing the cultures are summarized in Table 1.

TABLE 1
Origin and *Atm* status of mouse cells

<i>Atm</i> status	Mouse ID no.	Mouse strain	Sex
+/+	B-36	C57BL/6J	Male
+/+	B-70	C57BL/6J	Male
+/+	B-28	BALB/cByJ	Male
+/+	B-29	BALB/cByJ	Male
+/+	B-34	A/J	Male
+/+	B-42	A/J	Male
+/+	B-38	129S6	Male
+/+	B-58	129S6	Male
-/-	B-57	C57BL/6J	Female
-/-	B-68	C57BL/6J	Male
-/-	B-46	BALB/cByJ	Male
-/-	B-55	BALB/cByJ	Female
-/-	B-47	A/J	Male
-/-	B-49	A/J	Male
-/-	B-26	129S6	Male
-/-	B-41	129S6	Female

2.2.1. Cell culture

Fibroblast cultures were established from mouse ear from at least five mice of each mouse strain. Ears were washed with penicillin and streptomycin containing growth medium. The ear sample was cut with two sharp scalpels into smaller sample tissue pieces. These small tissue pieces were suspended in 15 ml centrifuge tube containing 2 U/ml of collagenase solution and digested on the shaker for 40 min. at 37°C. The fragments were washed three times with warm growth medium to remove collagenase. The pellets of the digested tissue were pipetted hard to obtain single cells or small tissue fragments before plating on tissue

culture dish. Fibroblasts were cultured in minimal essential medium (MEM) supplemented with 10% fetal bovine serum (FBS), 100 U/ml penicillin, and 100 µg/ml of streptomycin and maintained at 37°C in a humidified atmosphere of 5% CO₂ in air. These cells were synchronized and maintained after two days in a G₀/G₁ state during irradiation and using the isoleucine deprivation method (67).

2.2.2. Irradiation

Irradiations were carried out using either a J. L. Shepherd Model Mark I-68 222-TBq (6000 Ci) ¹³⁷Cs irradiator. The dose rate for the acute high-dose-rate exposure was 2.5 Gy/min at room temperature.

2.2.3. Metaphase chromosome preparation

Immediately after irradiation, the fibroblasts were sub-cultured and treated for 6 hours with colcemid prior to harvest. 0.1 µg/ml of colcemid (Invitrogen) was added to the media inside the flask of cells in order to capture the chromosomes in the first metaphase post-irradiation. The cells were then trypsinized and suspended in 75 mM KCl solution at 37°C in a water bath for 20 minutes. Each sample was fixed in Carnoy's solution (3:1 methanol to acetic acid) according to standard cytogenetic procedures (68). Before the cell solution was dropped, the slides were chilled in ice water. After application, the slides were set aside and allowed to air dry for approximately 5 minutes. For PNA FISH staining, once the slides were dry, they were immersed in 4% paraformaldehyde (PFA) in phosphate-buffered saline (PBS) for 10 minutes after which they were immediately washed with PBS and then immersed in 0.1 mg/ml of RNase A in PBS solution for 15 minutes at 37°C. The slides were then washed again with fresh PBS and placed in a solution prepared with 1% pepsin in 40 mL of 100 mM HCl at 37°C for 20 minutes. After, the slides were washed again in fresh PBS and then placed in an ethanol series for dehydration for 2 to 3 minutes each.

2.2.4. Modified PNA FISH method

After dehydration, hybridization was performed using a hybridization solution containing formamide, 200 nM of TelG-Cy3, 200 nM of CENPB Box-FAM (Panagene, Thousand Oaks, CA), 1M Tris-HCl, and pure water. 15 μ L of the staining solution was pipetted onto the slide and covered with a cover slip that contained rubber cement along the edges to create a firm seal over the stain and slide. The slides were then allowed to set overnight at room temperature after which the cover slip was removed and placed in PN buffer at 37°C for five minutes and then washed with freshly prepared PBS at room temperature. After washing, the slides were counterstained with DAPI in antifade (Invitrogen). Digital images were captured using a Zeiss Axioskop Microscope with CoolSnapHQ and Metamorph software. The slides were analyzed at 60X magnification to view and obtain pictures of stained centromere and telomere configurations as described below.

2.2.5. Scoring method for chromosome aberrations

Fluorescence images were captured using a Zeiss Axioskop microscope equipped with filters for observation of DAPI (blue), FITC (green), and TRITC (red). The total number of chromosomes per metaphase spread was counted and all aberrations were recorded. The observed aberrations include: Dicentric chromosomes, chromosomes with two centromeric signals. Acentric fragments which indicates loss of the centromere signal. Telomeric-associated fusions were classified based on presence of telomeric signals at the fusion site of the chromosome.

2.2.6. Statistical Analysis

Multiple comparisons among means for aberration formation frequencies were performed with a one-way ANOVA followed by Tukey's multiple comparison test on Prism Version 5.0c. Results were considered significantly different at $P < 0.05$.

2.3. RESULTS

A normalized aberration frequency was calculated for each *Atm*^{+/+} and *Atm*^{-/-} genotype per strain background as seen in Table 2. Frequencies of aberration formation for each cell strain were calculated per 50 metaphase cell spreads.

TABLE 2
Summary of aberration frequencies for C57BL/6J, BALB/cByJ, A/J and 129S6
Atm^{+/+} and *Atm*^{-/-} strain backgrounds

Gene Mutation	ATM Status	Mouse Cell Strain	Dose (Gy)	Metaphase analyzed	Average chromosome number per cell	Chromosome Fusion Event	Chromosome Telomeric Fusion Event	Frequency of Telomere-Associated Fusion per Total Fusion Event	Normalized Frequency of Dicentric Formation per cell	Normalized Frequency of acentric fragment per cell
B6	+/+	B-36	0	45	54.69	0	0	0	0	0
			1	50	52.86	4	0	0	0.061	0.008
			2	50	58.48	15	1	0.067	0.178	0.102
		B-70	0	50	77.70	0	0	0	0	0
			1	50	73.02	6	0	0	0.022	0.061
			2	46	73.61	29	0	0	0.307	0.200
B6	-/-	B-57	0	50	68.00	4	1	0.250	0.094	0
			1	49	73.51	39	3	0.077	0.333	0.342
			2	50	76.32	29	0	0	0.283	0.298
		B-68	0	50	64.58	6	2	0.333	0.074	0
			1	50	68.50	18	0	0	0.175	0.210
			2	50	70.90	61	8	0.131	0.609	0.604
BALB/c	+/+	B-28	0	50	56.10	0	0	0	0	0
			1	50	63.86	7	3	0.429	0.338	0.417
			2	40	55.68	8	0	0	0.162	0.365
		B-29	0	50	44.38	3	1	0.333	0.036	0
			1	45	40.71	2	0	0	0.022	0.197
			2	50	60.10	13	1	0.077	0.146	0.224
BALB/c	-/-	B-55	0	49	116.80	19	1	0.053	0.126	0
			1	50	101.04	58	3	0.052	0.435	0.281
			2	50	101.88	139	11	0.079	0.966	0.648
		B-46	0	50	89.38	10	0	0	0.090	0
			1	50	84.40	26	1	0.038	0.246	0.177
			2	50	81.44	73	3	0.041	0.639	0.673
AJ	+/+	B-42	0	50	83.58	0	0	0	0	0
			1	50	81.6	4	0	0	0.029	-0.008
			2	50	75.24	16	0	0	0.128	0.156
		B-34	0	50	75.02	0	0	0	0	0
			1	50	73.8	2	0	0	0.022	-0.014
			2	50	64.44	11	0	0	0.124	0.158
AJ	-/-	B-47	0	50	69.24	45	1	0.022	0.231	0
			1	50	71.76	63	1	0.016	0.468	0.409
			2	50	69.26	92	3	0.033	0.762	0.658
		B-49	0	50	62.14	9	0	0	0.103	0
			1	50	59.40	37	2	0.054	0.458	0.131
			2	48	60.58	30	0	0	0.330	0.147
129S6	+/+	B-38	0	40	75.85	1	0	0	0	0
			1	50	68.04	2	0	0	0.012	0.081
			2	24	59.71	3	0	0	0.084	0.054
		B-58	0	50	70.34	3	0	0	0.023	0
			1	50	62.46	11	0	0	0.128	0.088
			2	50	56.24	20	1	0.050	0.270	0.310
129S6	-/-	B-26	0	50	66.20	14	1	0.071	0.145	0
			1	50	41.50	7	1	0.143	0.116	0.127
			2	46	45.30	14	1	0.071	0.250	0.197
		B-41	0	50	83.58	26	1	0.038	0.134	0
			1	50	74.92	27	0	0	0.256	0.262
			2	50	70.12	69	5	0.072	0.582	0.838

The values were also normalized to 40 chromosomes per cell spread to account for the polyploidy and aneuploidy seen across most cell strains. There was no significant statistical difference observed in mean aberration frequency, for all chromosome-type aberrations, across a 0,1, and 2 Gy dose for each of the four mice strains with an *Atm*^{+/+} genotype, as shown in Figures 6, 7, and 8, as well as strains of the *Atm*^{-/-} genotype of 129S6.

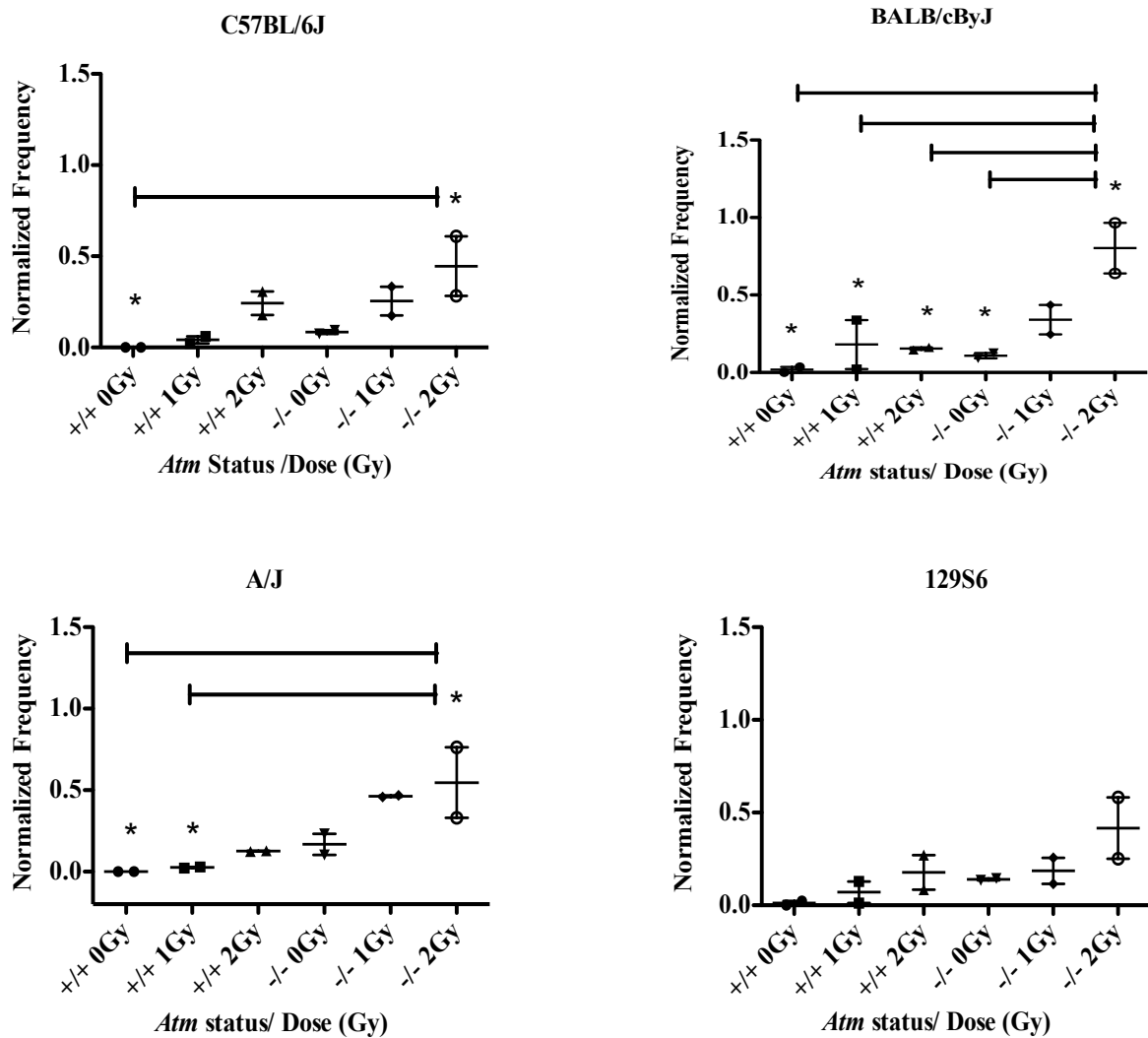


Figure 6. Comparison of normalized dicentric formation per metaphase over a 0, 1, and 2 Gy dose for each strain background of $Atm^{+/+}$ and $Atm^{-/-}$ genotypes. Error bars indicate standard errors of the mean. * indicates a statistically significant difference between $Atm^{+/+}$ cells and $Atm^{-/-}$ cells at $P < 0.05$.

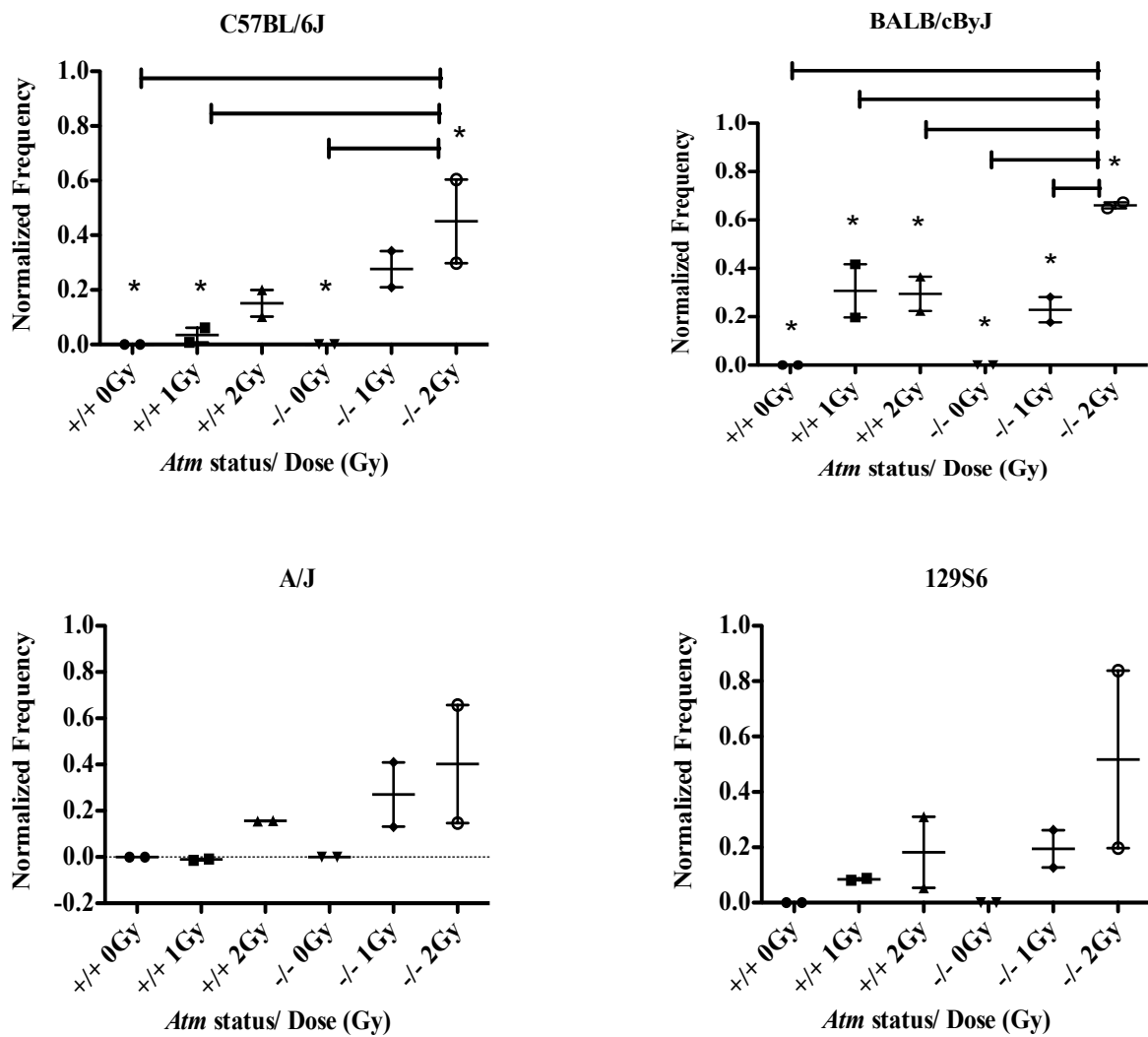


Figure 7. Comparison of normalized acentric fragment formation per metaphase over a 0, 1, and 2 Gy dose for each strain background of $Atm^{+/+}$ and $Atm^{-/-}$ genotypes. Error bars indicate standard errors of the mean. * indicates a statistically significant difference between $Atm^{+/+}$ cells and $Atm^{-/-}$ cells at $P < 0.05$.

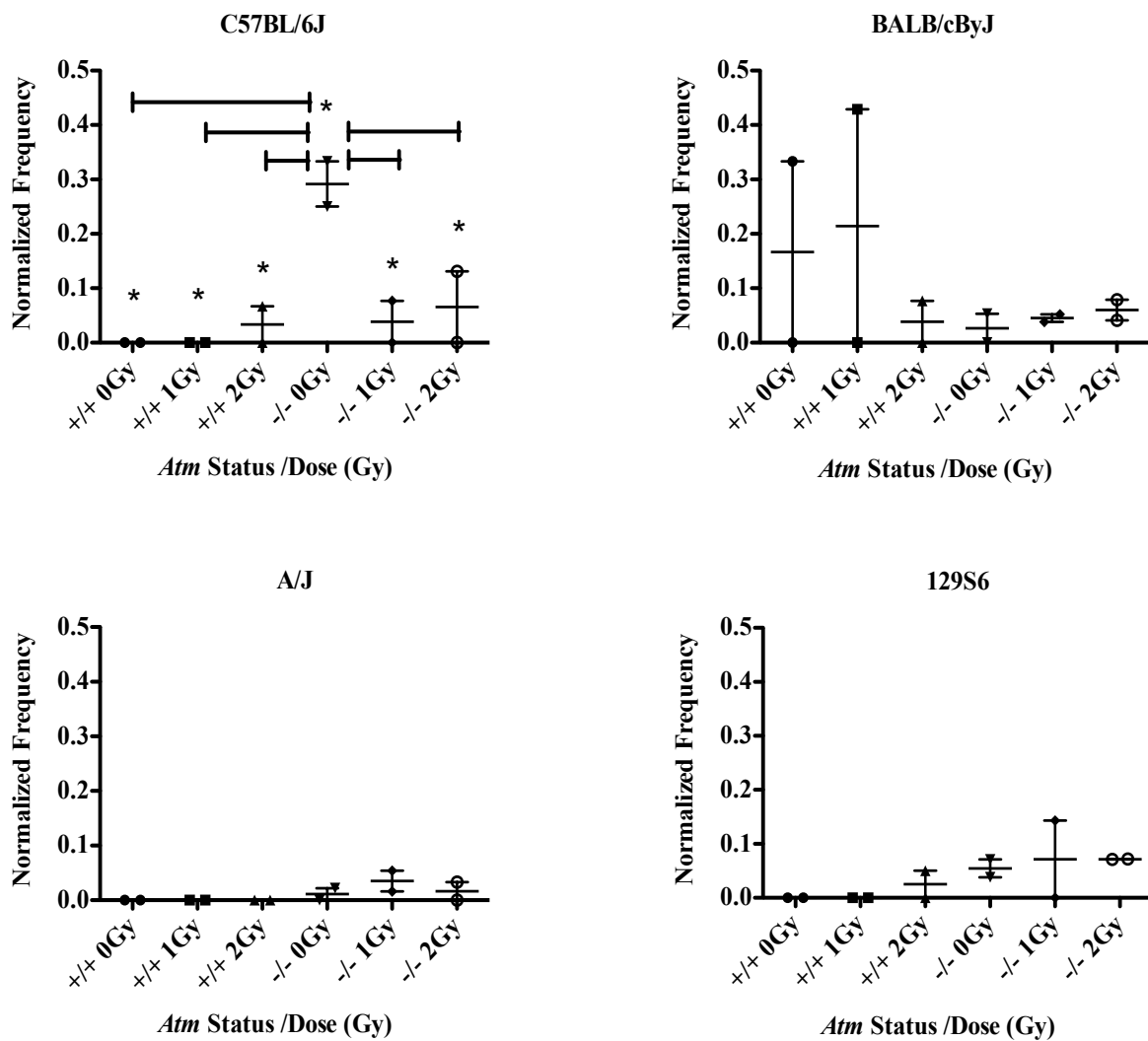


Figure 8. Comparison of normalized telomere-telomere fusion formation per metaphase over a 0, 1, and 2 Gy dose for each strain background of $Atm^{+/+}$ and $Atm^{-/-}$ genotypes. Error bars indicate standard errors of the mean. * indicates a statistically significant difference between $Atm^{+/+}$ cells and $Atm^{-/-}$ cells at $P < 0.05$.

There was a statistically significant elevation in acentric fragments and telomere-associated fusions in *Atm*^{-/-} strains from a 0 to 2 Gy dose for the C57BL/6J strain ($P= 0.0213$, $P= 0.0107$ respectively). Furthermore, the BALB/cByJ strain showed a statistically significant increase in average dicentric and acentric fragment yield across a 0 to 2 Gy dose for the *Atm*^{-/-} genotype ($P= 0.0132$, $P= 0.0015$ respectively).

2.4. DISCUSSION

The C57BL/6J *Atm*^{-/-} strains showed the greatest sensitivity due to the significant difference in every chromosome aberration type when compared to *Atm*^{+/+} strains of the same strain background. In addition, there was a heightened dose response effect over a 0-2 Gy dose for the C57BL/6J *Atm*^{-/-} strains for average acentric fragment and telomere-associated fusion yield. The BALB/cByJ mice strains also exhibited a dose response effect for the *Atm*^{-/-} genotype in average acentric fragment and dicentric yield, but when comparing *Atm*^{+/+} and *Atm*^{-/-} strains, there was only an increase in average dicentric frequency which suggests a lack of synergism between the loss of *Atm* and DNA-PKcs activity. The 129S6 and A/J strains yielded a similar radiosensitivity, however, the 129S6 knockouts were the only strains that showed an increase in telomere-associated fusion frequency. Collectively, the *Atm*^{-/-} genotypes for all inbred strain backgrounds exhibited a greater radiosensitivity through the increased frequency of chromosome-type aberration formation, however, the differing strain backgrounds determined whether that increase was dose-dependent. Therefore, an important consideration is that *ATM* status as well as the natural genetic variation of the inbred cell strain background provides diverse effects to DNA DSB repair and processing. This assay may provide a means of identifying and studying how radiosensitivity can be attributed, not only to genetic background, but also in variations among the background of the individual.

CHAPTER THREE

Induction of Chromosomal Aberrations Consequent to *Aspm* Excision Via the Cre-Lox Recombination System

3.1. BACKGROUND

A study by Fujimori et al. revealed a gene whose expression contributes to the maintenance and proper symmetric division of neuronal progenitors. The authors demonstrated, through HiCEP (high-coverage expression profiling), that after exposure to carbon and X-rays, the expression of the *ASPM* gene is downregulated in human and murine tissue culture cells (42). In another study done by Kato et. al. to further understand the role of *ASPM* on radiosensitivity, the authors were able to down-regulate *ASPM* through siRNA (small interfering RNA) in order to observe cellular sensitivity to irradiation as well as other clastogenic agents such as hydrogen peroxide, camptothecin, or cisplatin with the use of three different immortalized cell lines, U87MG glioblastoma cells, AG1521 human fibroblasts, and HeLa cervical carcinoma cells. Interestingly, the two tumor cell lines showed a greater sensitization versus the normal fibroblasts, which suggest a tumor targeting means of radiotherapy. Upon further examination, the mechanism of radiosensitivity through knockdown of *ASPM* with siRNA was through the inhibition of DNA DSB repair, specifically through the NHEJ pathway by using DNA-PKcs deficient human cells. Furthermore, PNA FISH techniques were used to monitor the effects of impaired DNA DSBs through the formation of IR-induced chromosomal aberrations in normal fibroblasts. Chromosomal translocations and breaks were seen after irradiation the cells in the G₀/G₁ stage of the cell cycle. Confirmation in the reduction of DNA double-strand break repair in cells through the NHEJ pathway was gained as well as the linear increase in the number of aberrations in *ASPM* knockdown cells (69). These studies clearly recognize the *ASPM* gene as important to chromosomal integrity. Therefore, we hypothesized that over a 48-hour time

period, conditional knockout MEF strains, *Aspm*^{-/-} will exhibit an increase in chromosomal sensitivity observed as chromosome-type aberrations. In order to observe these changes in cellular sensitivity, we were able to monitor chromosomal aberration formation through a modified PNA FISH technique.

3.2. MATERIALS AND METHODS

For this project, tamoxifen, in the absence of radiation, was used to create a series of MEF cell lines with variations in floxed alleles for the *ASPM* gene via Cre-lox site-specific recombination. The Cre-lox site-specific recombination system involves an inducible gene targeting method, such as the enzymatic activity of the Cre recombinase, to specifically and efficiently modify DNA sequences flanked by loxP sites, 34-bp sequences composed of two 13-bp inverted repeats separated by an asymmetric 8-bp core sequence (Figure 9). Modifications can result in inversion, deletion, or translocation of the loxP sites depending on their orientation as diagrammed in Figure 10.

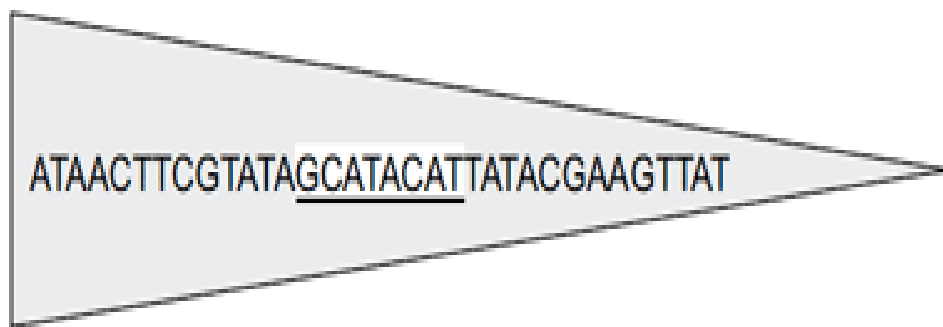


Figure 9. The loxP sequence. The underlined sequence is the 8-bp core sequence where recombination takes place. The core sequence is flanked by two inverted repeats (70).

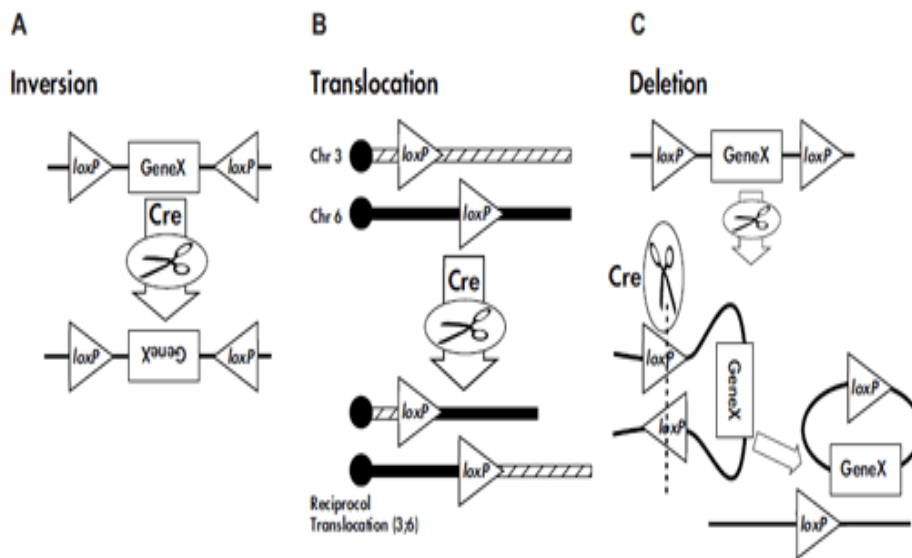


Figure 10. Diagram representing variations of the Cre-lox recombination system. The different outcomes of a recombination event are determined by the orientation and location of the loxP sites. (A) Inversion occurs when the loxP sites are oriented in opposing directions. (B) Chromosomal translocation results when the loxP sites are located on different chromosomes. (C) Deletion results when the loxP sites are oriented in the same direction on a chromosome segment (70).

The particular Cre-lox system used in this experiment is tamoxifen-inducible where by fusing the Cre recombinase to a mutant ligand-binding domain of the estrogen receptor (ER), the chimeric recombinase activity in the cultured cells of the transgenic mouse is then dependent on the presence of the synthetic ligands, tamoxifen and 4-hydroxytamoxifen, but not endogenous estrogen (71, 72). Upon the addition of tamoxifen, the fusion protein is transported to the nucleus for the excision of one or both floxed alleles of the *ASPM* gene.

3.2.1. Cell culture

Mouse embryonic fibroblasts (MEFs) were prepared from day 14.5 mouse embryo and cultured in minimal essential medium (MEM) with 10% fetal bovine serum (FBS) and 1% penicillin maintained at 37°C in a humidified atmosphere of 5% CO₂ in air. Genotypes were determined by quantitative RT-PCR using tissue from the heads of the embryo using primers specific for the murine *Aspm* (Table 3). All MEF cultures had a similar passage range between two and five. All experimental protocols involving mice were reviewed and approved by the Animal Care and Use Committee of the National Institute of Radiological Sciences (NIRS), and the experiments were performed in strict accordance with the NIRS Guidelines for the Care and Use of Laboratory Animals.

TABLE 3
Origin and *Aspm* status of mouse cells

<i>Aspm</i> genotype	MEF ID no.	Cre Activity	<i>Aspm</i> genotype (Post Tamoxifen addition)
F/F	1	-	F/F
F/F	2	+	-/-
+/F	3	-	+/F
+/F	4	-	+/F
+/F	5	+	+/-
F/F	6	+	-/-
+/F	7	+	+/-
+/F	10	+	+/-
F/F	15	+	-/-

3.2.2. Metaphase chromosome preparation

Each of the nine MEF cell cultures were grown to confluency in T25 flasks, then sub-cultured where the media of each flask was spiked with 0.2 μ M tamoxifen in ethanol prior to colcemid addition. 0.1 μ g/ml of colcemid (Invitrogen) was added to the media inside the flask of cells six hours prior to harvesting of chromosomes at time periods of 24 and 48 hours post-tamoxifen addition. The cells were then trypsinized and suspended in 75 mM KCl solution at 37°C in a water bath for 20 minutes. Each sample was fixed in Carnoy's solution (3:1 methanol to acetic acid) according to standard cytogenetic procedures (68). Before the cell solution was dropped, the slides were chilled in ice water. After application, the slides were set aside and allowed to air dry for approximately 5 minutes. For PNA FISH staining, once the slides were dry, they were immersed in 4% PFA in PBS for 10 minutes after which they were immediately washed with PBS and then immersed in 0.1 mg/ml of RNase A in PBS solution for 15 minutes at 37°C. The slides were then washed again with fresh PBS and placed in a solution prepared with 1% pepsin in 40 ml of 100 mM HCl at 37°C for 20 minutes. After, the slides were washed again in fresh PBS and then placed in an ethanol series for dehydration for 2 to 3 minutes each.

3.2.3. Modified PNA FISH method

After dehydration, hybridization was performed using a hybridization solution containing 60% formamide, 200 nM of TelG-Cy3, 200 nM of CENPB Box-FAM (Panagene, Thousand Oaks, CA), 1M Tris-HCl, and pure water. 15 μ L of the staining solution was pipetted onto the slide and covered with a cover slip that contained rubber cement along the edges to create a firm seal over the stain and slide. The slides were then allowed to set overnight at room temperature after which the cover slip was removed and placed in PN buffer at 37°C for five minutes and then washed with freshly prepared PBS at room temperature. After washing, the slides were counterstained with DAPI in antifade (Invitrogen). Digital images were captured

using a Zeiss Axioskop Microscope with CoolSnapHQ and Metamorph software. The slides were analyzed at 60X magnification to view and obtain pictures of stained centromere and telomere configurations as described below.

3.2.4. Scoring method for chromosome aberrations

As stated previously, fluorescence images were captured using a Zeiss Axioskop microscope equipped with filters for observation of DAPI (blue), FITC (green), and TRITC (red). The total number of chromosomes per metaphase spread was counted and all aberrations were recorded. The observed aberrations include: Dicentric chromosomes, chromosomes with two centromeric signals. Acentric fragments, or induced complete loss, which indicates loss of the centromere signal.

3.2.5. Statistical Analysis

Multiple comparisons among means for aberration formation frequencies were performed with a one-way ANOVA followed by Tukey's multiple comparison test on Prism Version 5.0c. Results were considered significantly different at $P < 0.05$.

3.3. RESULTS

For each cell strain and chromosome-type aberration, the frequency of formation was calculated per 50 metaphase chromosome spreads and then normalized to 40 chromosomes per metaphase spread to account for polyploidy and aneuploidy. The cell strains were then grouped by *Aspm* genotype status and an average frequency of each aberration formed was calculated as shown in Table 4.

TABLE 4
Summary of aberration frequencies for MEF strains across differing *Aspm* genotypes

<i>Aspm</i> Genotype post-Tamoxifen addition	MEF ID	Time (hr)	Metaphase analyzed	Average chromosome number per cell	Normalized Frequency of Dicentric Formation per cell	Normalized Frequency of acentric fragment per cell
<i>Aspm</i> ^{F/F}	MEF 1	0	50	61.48	0	0
		24	50	51.74	0.046	0.031
		48	50	55.78	0.014	0.043
<i>Aspm</i> ^{+/F}	MEF 3	0	50	69.76	0.000	0.998
		24	50	44.52	0.072	2.102
		48	45	43.8	0	0.649
	MEF 4	0	48	55.67	0	0.898
		24	48	51.27	0	1.008
		48				
<i>Aspm</i> ^{+/-}	MEF 5	0	49	47.88	0.017	0.034
		24	50	49.46	0.065	1.844
		48	50	51.82	0.185	1.497
	MEF 7	0	43	38.88	0	1.005
		24	47	52.55	0	1.781
		48				
	MEF 10	0	49	55.57	0	1.204
		24	50	51.5	0.062	2.439
		48	32	46.00	0.163	1.359
<i>Aspm</i> ^{-/-}	MEF 2	0	50	51.98	0.031	1.28
		24	50	62.08	0.180	2.977
		48	45	45.27	0.098	1.591
		0	50	51.90	0.015	0.971
		24	47	52.55	0.015	2.072
		48				
	MEF 6	0	50	57.55	0	0.965
		24	50	56.84	0.014	0.915
		48				
	MEF 15	0	50	65.22	0.024	0.037
		24	50	53.26	0	1.127
		48	33	70.55	0.412	2.320

A slight increase in dicentric formation was seen across *Aspm*^{+/+}, *Aspm*^{+/-}, and *Aspm*^{-/-} genotypes over 24-hours post-tamoxifen addition in comparison to the control, or untreated cells. However, over 48-hours, a more pronounced increase in dicentric formation was observed for the conditional knockout cell strains (Figure 11). A greater increase in acentric fragment yield was observed over cell lines of the *Aspm*^{+/-} and *Aspm*^{-/-} genotype over a 48-hour time period, although a greater elevation was observed in *Aspm*^{+/-} over a 24-hour time period (Figure 12). However, the increases seen between the *Aspm*^{+/-} and *Aspm*^{-/-} genotypes were not statistically different.

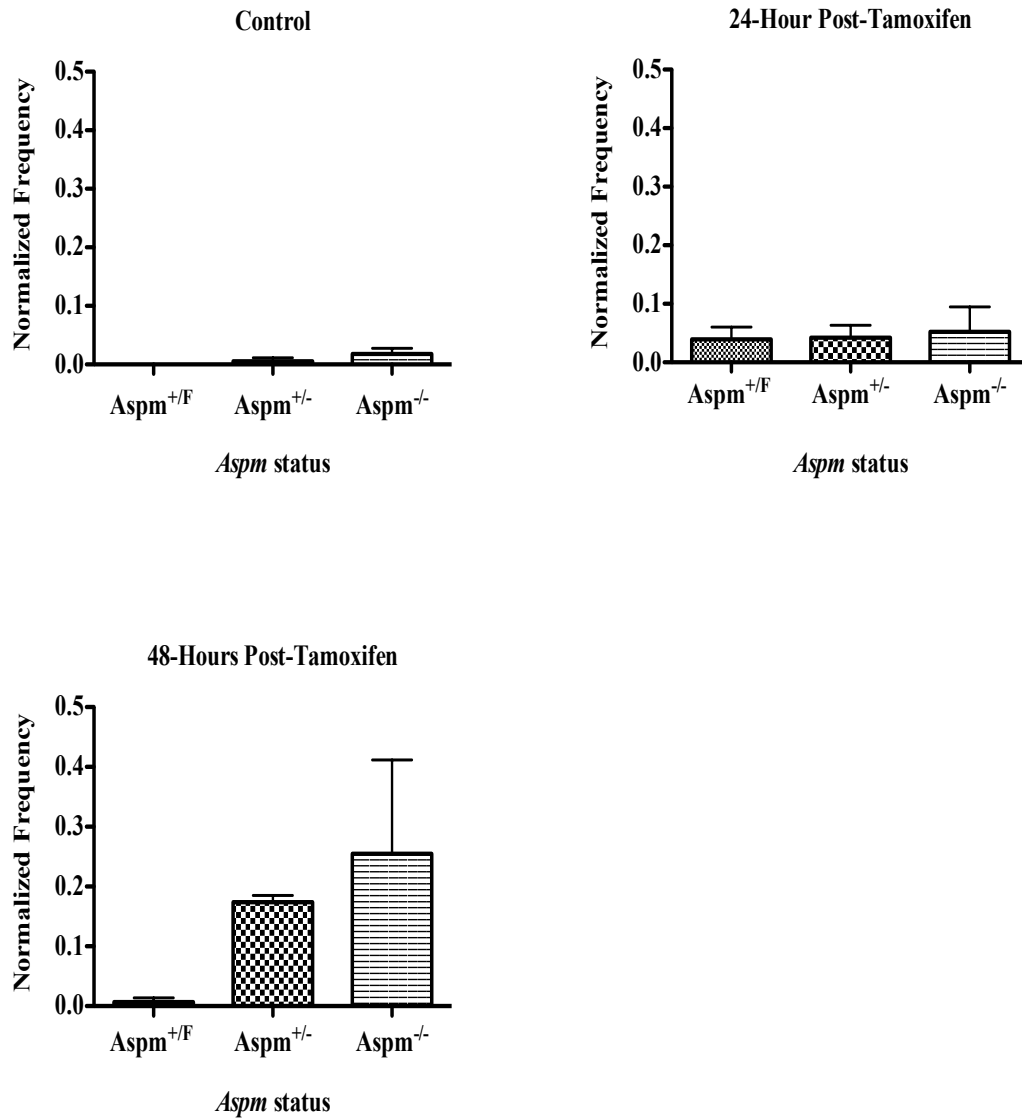


Figure 11. Average dicentric formation per metaphase at 24 and 48-hours post-tamoxifen addition compared to control (untreated) frequencies. MEF cell lines were grouped according to *Aspm* status. MEF cell lines that were not included in the 48-hour time period are MEF 4, 6, and 7. Error bars indicate standard errors of the mean.

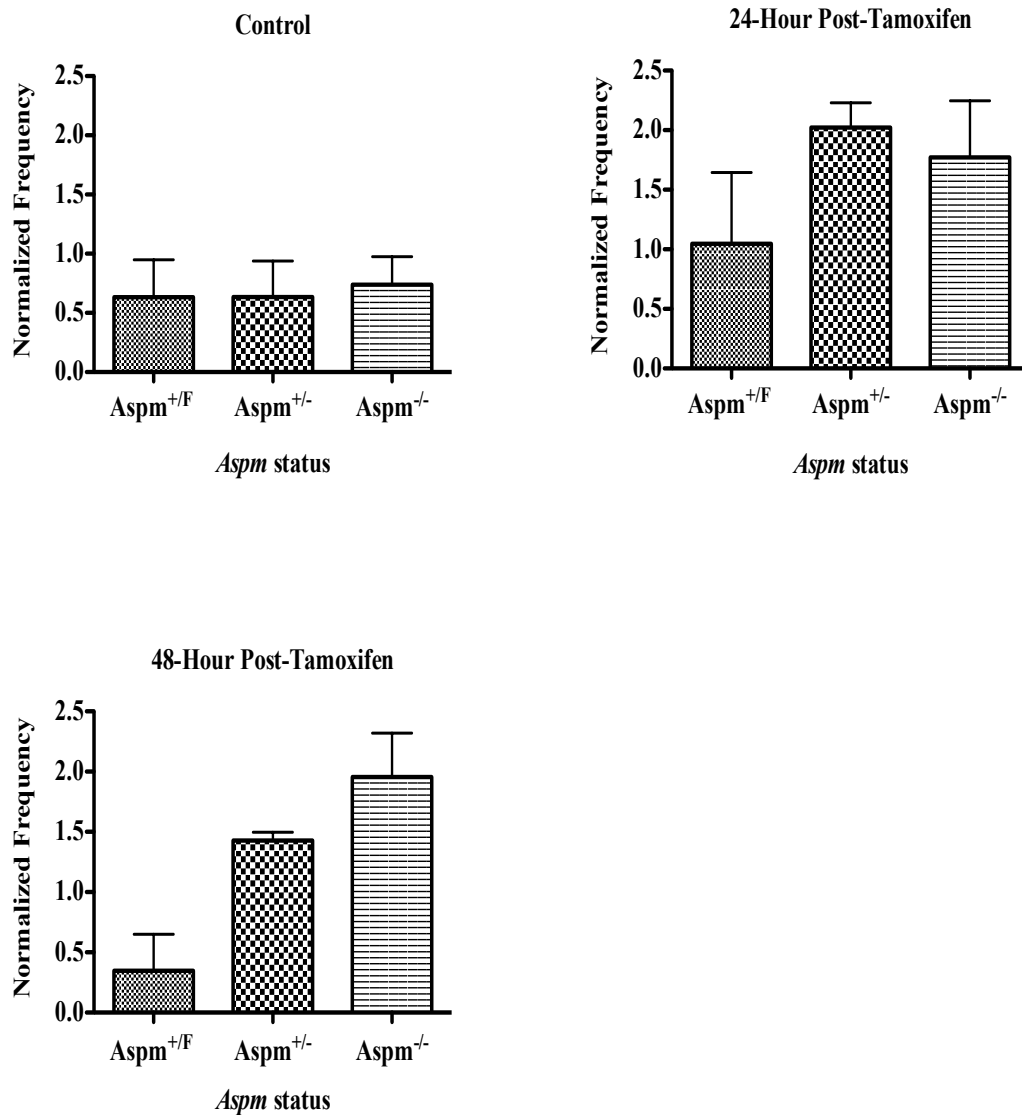


Figure 12. Average acentric fragment formation per metaphase at 24 and 48-hours post-tamoxifen addition compared to control (untreated) frequencies. MEF cell lines were grouped according to *Aspm* status. MEF cell lines that were not included in the 48-hour time period are MEF 4, 6, and 7. Error bars indicate standard errors of the mean.

3.4. Discussion

This study utilized a conditional knockout model, via the Cre-lox recombination system, where MEFs of the conditional knockout genotype led to an increase in DSBs, observed as dicentric and acentric fragment formation, as early as 24 hours post-tamoxifen addition. Interestingly, the heterozygous *Aspm* genotype also exhibited an increase in acentric fragment and dicentric formation over a 24-hour time period. The frequency of average dicentric yield was comparable, than cell strains of the *Aspm*^{-/-} genotype at 24-hours, and even surpassed the *Aspm*^{-/-} strains in average acentric fragment formation at 24-hours. However, since no statistical differences were observed between the *Aspm*^{+/-} and *Aspm*^{-/-} cells, a possible pathogenic mechanism is haploinsufficiency where a single functional copy of a gene is insufficient to maintain normal function (73). Frequently, organisms that are heterozygous for a loss-of-function allele exhibit a normal phenotype due to the presence of one wild-type allele which masks any phenotypic consequences due to a redundancy of cellular physiology (74). Biochemical studies provide a possible explanation when a reduced fitness in these heterozygous strains is observed which states that a balance of protein levels are required to maintain cytoskeletal integrity (75). In agreement with the experimental work by Kato et. al. where a suppression of the *Aspm* gene via siRNA, increased radiosensitization as well as impairs DNA double-strand break repair (69). The observations presented in this study suggest a possible underlying mechanism for the onset of microcephaly where chromosomal instability consequent to mutations in the *ASPM* gene promotes an increase in DNA DSBs, and with the impairment of proper repair mechanisms, will result in a disruption of crucial cellular mechanisms involved in proper neurogenesis.

CHAPTER FOUR

CONCLUSIONS

In conclusion, DNA damage, through SSBs or DSBs, resulting in chromosomal instability is a crucial component in cancer research. Due to the complex nature of the scope, it is ideal to have methods and assays in place that provide a quick and simple way for the detection of such alterations of the genome. The modified PNA FISH technique has provided a quick and efficient method in cytogenetic analysis. This method has been simplified from previous adaptations of radiolabeling, denaturation, and synthetic dye applications, which are more error prone and less distinctive of molecular structures. This was exemplified in the *Atm* experiment where telomere-associated fusions could be definitively verified quickly upon location of the red interstitial telomere signal on a blue DAPI background. Thus, through this easily identifiable method, we were able to classify and differentiate chromosome-type aberrations for four inbred mouse strains with differing genetic backgrounds of either *Atm*^{+/+} or *Atm*^{-/-}. The comparative evidence that was provided here has confirmed the necessity of the *Atm* protein in the NHEJ DNA repair pathway, when a statistically significant increase in dicentric and acentric fragment aberrations was seen in *Atm*^{-/-} strains across three of the four backgrounds: A/J, 129S6, and C57BL/6J, although this response was not dose-dependent. Another interesting result was seen in the BALB/cByJ strain, with a known *Prkdc* defect, where there was no synergistic affect and the *Atm*^{+/+} and *Atm*^{-/-} replicative strains did not show any differences in average aberration frequencies. Therefore, with the absence of the *Atm* gene, as seen in the A-T phenotype, there is an increase in radiosensitivity among these strain backgrounds, which is an important aspect when using these models for studying A-T. We were also able to classify aberrations across differing *Aspm* genotypes in MEF cell lines. Through the Cre-lox recombination system, we were able to observe an increased sensitivity in conditional knockout strains in comparison to

untreated controls over a 24 and 48 hour time period. This further corroborates the study of Kato et. al. where when *Aspm* is suppressed, there is an elevation in chromosomal instability as seen through an increase in DNA DSBs. It was also shown in this experiment, that there is a prominent increase in sensitivity of the heterozygous genotype, which is characteristic of haploinsufficiency, and that *Aspm* is an essential component not only for neuronal development but in DNA repair regulation and/or maintenance.

REFERENCES

1. Bedford JS & Dewey WC (2002) Radiation Research Society. 1952-2002. Historical and current highlights in radiation biology: has anything important been learned by irradiating cells? *Radiat Res* 158(3): 251-291.
2. Morgan WF, Day JP, Kaplan MI, McGhee EM, & Limoli CL (1996) Genomic instability induced by ionizing radiation. *Radiat Res* 146(3): 247-258.
3. Jeggo PA (1998) Identification of genes involved in repair of DNA double-strand breaks in mammalian cells. *Radiat Res* 150(5 Suppl): S80-91.
4. Bender MA, *et al.* (1988) Current status of cytogenetic procedures to detect and quantify previous exposures to radiation. *Mutat Res* 196(2): 103-159.
5. Ward JF (1995) Radiation mutagenesis: the initial DNA lesions responsible. *Radiat Res* 142(3): 362-368.
6. Limoli CL, Kaplan MI, Phillips JW, Adair GM, & Morgan WF (1997) Differential induction of chromosomal instability by DNA strand-breaking agents. *Cancer Res* 57(18): 4048-4056.
7. Muller HJ (1927) Artificial Transmutation of the Gene. *Science* 66(1699): 84-87.
8. Savage JR (1975) Classification and relationships of induced chromosomal structural changes. *J Med Genet* 13: 103-122.
9. Choo KHA (1997) The Centromere. *Oxford University Press*: 320.
10. Ohzeki J, Nakano M, Okada T, & Masumoto H (2002) CENP-B box is required for de novo centromere chromatin assembly on human alphoid DNA. *J Cell Biol* 159(5): 765-775.
11. Wu L, *et al.* (2006) Pot1 deficiency initiates DNA damage checkpoint activation and aberrant homologous recombination at telomeres. *Cell* 126(1): 49-62.
12. Sachs RK, Chen AM, & Brenner DJ (1997) Review: proximity effects in the production of chromosome aberrations by ionizing radiation. *Int J Radiat Biol* 71(1): 1-19.

13. de Lange T (2005) Shelterin: the protein complex that shapes and safeguards human telomeres. *Gene Dev* 19(18): 2100-2110.
14. Zakian VA (1995) Telomeres: beginning to understand the end. *Science* 270(5242): 1601-1607.
15. Christmann M, Tomicic MT, Roos WP, & Kaina B (2003) Mechanisms of human DNA repair: an update. *Toxicology* 193(1-2): 3-34.
16. Takata M, *et al.* (1998) Homologous recombination and non-homologous end-joining pathways of DNA double-strand break repair have overlapping roles in the maintenance of chromosomal integrity in vertebrate cells. *Embo J* 17(18): 5497-5508.
17. Sonoda E, Hohegger H, Saberi A, Taniguchi Y, & Takeda S (2006) Differential usage of non-homologous end-joining and homologous recombination in double strand break repair. *DNA Repair (Amst)* 5(9-10): 1021-1029.
18. McKinnon PJ (2004) ATM and ataxia telangiectasia. *EMBO reports* 5(8): 772-776.
19. Lavin MF, *et al.* (2005) ATM signaling and genomic stability in response to DNA damage. *Mutat Res* 569(1-2): 123-132.
20. Bosotti R, Isacchi A, & Sonnhammer EL (2000) FAT: a novel domain in PIK-related kinases. *Trends in biochemical sciences* 25(5): 225-227.
21. Kouprina N, *et al.* (2004) Accelerated evolution of the ASPM gene controlling brain size begins prior to human brain expansion. *PLoS Biol* 2(5): E126.
22. Bond J, *et al.* (2002) ASPM is a major determinant of cerebral cortical size. *Nat Genet* 32(2): 316-320.
23. National Institutes of Health (2011) ASPM. (U.S. National Library of Medicine).
24. Shiloh Y (2003) ATM and related protein kinases: safeguarding genome integrity. *Nature reviews. Cancer* 3(3): 155-168.
25. Riballo E, *et al.* (2004) A pathway of double-strand break rejoining dependent upon ATM, Artemis, and proteins locating to gamma-H2AX foci. *Mol Cell* 16(5): 715-724.

26. Chun HH & Gatti RA (2004) Ataxia-telangiectasia, an evolving phenotype. *DNA Repair (Amst)* 3(8-9): 1187-1196.
27. Pecker I, *et al.* (1996) Identification and chromosomal localization of Atm, the mouse homolog of the ataxia-telangiectasia gene. *Genomics* 35(1): 39-45.
28. Barlow C, *et al.* (1996) Atm-deficient mice: a paradigm of ataxia telangiectasia. *Cell* 86(1): 159-171.
29. Higgins J, *et al.* (2010) Human ASPM participates in spindle organisation, spindle orientation and cytokinesis. *BMC Cell Biol* 11: 85.
30. Kouprina N, *et al.* (2005) The microcephaly ASPM gene is expressed in proliferating tissues and encodes for a mitotic spindle protein. *Hum Mol Genet* 14(15): 2155-2165.
31. Fish JL, Kosodo Y, Enard W, Paabo S, & Huttner WB (2006) Aspm specifically maintains symmetric proliferative divisions of neuroepithelial cells. *Proc Natl Acad Sci U S A* 103(27): 10438-10443.
32. Lin SY, *et al.* (2008) ASPM is a novel marker for vascular invasion, early recurrence, and poor prognosis of hepatocellular carcinoma. *Clin Cancer Res* 14(15): 4814-4820.
33. Riparbelli MG, Callaini G, Glover DM, & Avides Mdo C (2002) A requirement for the Abnormal Spindle protein to organise microtubules of the central spindle for cytokinesis in *Drosophila*. *J Cell Sci* 115(Pt 5): 913-922.
34. Jackson AP, *et al.* (2002) Identification of microcephalin, a protein implicated in determining the size of the human brain. *Am J Hum Genet* 71(1): 136-142.
35. Ripoll P, Pimpinelli S, Valdivia MM, & Avila J (1985) A cell division mutant of *Drosophila* with a functionally abnormal spindle. *Cell* 41(3): 907-912.
36. do Carmo Avides M, Tavares A, & Glover DM (2001) Polo kinase and Asp are needed to promote the mitotic organizing activity of centrosomes. *Nat Cell Biol* 3(4): 421-424.
37. Bond J, *et al.* (2003) Protein-truncating mutations in ASPM cause variable reduction in brain size. *Am J Hum Genet* 73(5): 1170-1177.
38. Aicardi J (1998) *Malformations of the central nervous system* (Mac Keith, London) 2 Ed.

39. Pulvers JN, *et al.* (2010) Mutations in mouse *Aspm* (abnormal spindle-like microcephaly associated) cause not only microcephaly but also major defects in the germline. *Proc Natl Acad Sci U S A* 107(38): 16595-16600.
40. Ishida Y, *et al.* (2006) Dose-response and large relative biological effectiveness of fast neutrons with regard to mouse fetal cerebral neuron apoptosis. *J Radiat Res* 47(1): 41-47.
41. Blaschke AJ, Staley K, & Chun J (1996) Widespread programmed cell death in proliferative and postmitotic regions of the fetal cerebral cortex. *Development* 122(4): 1165-1174.
42. Fujimori A, *et al.* (2008) Ionizing radiation downregulates ASPM, a gene responsible for microcephaly in humans. *Biochem Biophys Res Commun* 369(3): 953-957.
43. Geard CR (1992) Cytogenetic assays for genotoxic agents. *Lens Eye Toxic Res* 9(3-4): 413-428.
44. Fenech M (2008) The micronucleus assay determination of chromosomal level DNA damage. *Methods Mol Biol* 410: 185-216.
45. Wilson DM, 3rd & Thompson LH (2007) Molecular mechanisms of sister-chromatid exchange. *Mutat Res* 616(1-2): 11-23.
46. Hittelman WN & Rao PN (1975) The nature of adriamycin-induced cytotoxicity in Chinese hamster cells as revealed by premature chromosome condensation. *Cancer Res* 35(11 Pt 1): 30-27-35.
47. Cornforth MN & Bedford JS (1985) On the nature of a defect in cells from individuals with ataxia-telangiectasia. *Science* 227(4694): 1589-1591.
48. Levisky JM & Singer RH (2003) Fluorescence in situ hybridization: past, present and future. *J Cell Sci* 116(Pt 14): 2833-2838.
49. Rudkin GT & Stollar BD (1977) High resolution detection of DNA-RNA hybrids in situ by indirect immunofluorescence. *Nature* 265(5593): 472-473.
50. Gall JG & Pardue ML (1969) Formation and detection of RNA-DNA hybrid molecules in cytological preparations. *Proc Natl Acad Sci U S A* 63(2): 378-383.

51. Bauman JG, Wiegant J, Borst P, & van Duijn P (1980) A new method for fluorescence microscopical localization of specific DNA sequences by in situ hybridization of fluorochromelabelled RNA. *Exp Cell Res* 128(2): 485-490.
52. Kislauskis EH, Li Z, Singer RH, & Taneja KL (1993) Isoform-specific 3'-untranslated sequences sort alpha-cardiac and beta-cytoplasmic actin messenger RNAs to different cytoplasmic compartments. *J Cell Biol* 123(1): 165-172.
53. Hada M, Cucinotta FA, Gonda SR, & Wu H (2007) mBAND analysis of chromosomal aberrations in human epithelial cells exposed to low- and high-LET radiation. *Radiat Res* 168(1): 98-105.
54. Yurov YB, *et al.* (1996) High resolution multicolor fluorescence in situ hybridization using cyanine and fluorescein dyes: rapid chromosome identification by directly fluorescently labeled alphoid DNA probes. *Hum Genet* 97(3): 390-398.
55. Yan J, Chen BZ, Bouchard EF, & Drouin R (2004) The labeling efficiency of human telomeres is increased by double-strand PRINS. *Chromosoma* 113(4): 204-209.
56. Nielsen PE, Egholm M, Berg RH, & Buchardt O (1991) Sequence-selective recognition of DNA by strand displacement with a thymine-substituted polyamide. *Science* 254(5037): 1497-1500.
57. Egholm M, Buchardt O, Nielsen PE, & Berg RH (1992) Peptide Nucleic-Acids (Pna) - Oligonucleotide Analogs with an Achiral Peptide Backbone. *J Am Chem Soc* 114(5): 1895-1897.
58. Chen C, Hong YK, Ontiveros SD, Egholm M, & Strauss WM (1999) Single base discrimination of CENP-B repeats on mouse and human Chromosomes with PNA-FISH. *Mamm Genome* 10(1): 13-18.
59. Czepulkowski B (2001) *Analyzing Chromosomes* (BIOS Scientific Publishers Limited London, UK).
60. Kato TA, *et al.* (2009) Variations in radiosensitivity among individuals: a potential impact on risk assessment? *Health Phys* 97(5): 470-480.
61. Kato TA, *et al.* (2006) gamma-H2AX foci after low-dose-rate irradiation reveal atm haploinsufficiency in mice. *Radiat Res* 166(1 Pt 1): 47-54.
62. Okayasu R, *et al.* (2000) A deficiency in DNA repair and DNA-PKcs expression in the radiosensitive BALB/c mouse. *Cancer Res* 60(16): 4342-4345.

63. Bogen KT & Witschi H (2002) Lung tumors in A/J mice exposed to environmental tobacco smoke: estimated potency and implied human risk. *Carcinogenesis* 23(3): 511-519.
64. Sundberg JP, Hanson CA, Roop DR, Brown KS, & Bedigian HG (1991) Myoepitheliomas in Inbred Laboratory Mice. *Vet Pathol* 28(4): 313-323.
65. Barlow C, *et al.* (1996) Atm-deficient mice: A paradigm of ataxia telangiectasia. *Cell* 86(1): 159-171.
66. Genik PC, Bielefeldt-Ohmann, H., Liu, x., Story, M.D., Ding, L., Bush, J., Fallgren, C., Weil, M.M. (Strain background determines lymphoma incidence in Atm knockout mice. Manuscript (Colorado State University, Fort Collins).
67. Tobey RA & Ley KD (1971) Isoleucine-Mediated Regulation of Genome Replication in Various Mammalian Cell Lines. *Cancer Res* 31(1):46-51.
68. Cartwright IM, Genet MD, & Kato TA (2013) A simple and rapid fluorescence in situ hybridization microwave protocol for reliable dicentric chromosome analysis. *J Radiat Res* 54(2): 344-348.
69. Kato TA, Okayasu R, Jeggo PA, & Fujimori A (2011) ASPM influences DNA double-strand break repair and represents a potential target for radiotherapy. *Int J Radiat Biol* 87(12): 1189-1195.
70. Nagy A (2000) Cre recombinase: the universal reagent for genome tailoring. *Genesis* 26(2): 99-109.
71. Feil R, *et al.* (1996) Ligand-activated site-specific recombination in mice. *Proc Natl Acad Sci U S A* 93(20): 10887-10890.
72. Sauer B (1987) Functional expression of the cre-lox site-specific recombination system in the yeast *Saccharomyces cerevisiae*. *Mol Cell Biol* 7(6): 2087-2096.
73. Huang N, Lee I, Marcotte EM, & Hurles ME (2010) Characterising and predicting haploinsufficiency in the human genome. *PLoS Genet* 6(10): e1001154.
74. Kacser H & Burns JA (1981) The molecular basis of dominance. *Genetics* 97(3-4): 639-666.

75. Deutschbauer AM, *et al.* (2005) Mechanisms of haploinsufficiency revealed by genome-wide profiling in yeast. *Genetics* 169(4): 1915-1925.
76. Ijichi K, *et al.* (1996) Inhibitory effect of 4-(2, 6-dichlorophenyl)-1, 2, 5-thiadiazol-3-yl-N-methyl, N-ethylcarbamate on replication of human immunodeficiency virus type 1 and the mechanism of action. *Biochem Mol Biol Int* 39(1): 41-52.

APPENDIX I

MODIFIED PNA FISH PROTOCOL

Traditionally, FISH techniques required the denaturation of target DNA for the successful hybridization of the molecular probe to complementary DNA sequences. The denaturing process required the use of formamide and salt solutions, which lower the temperature at which the DNA denatures to preserve the structural integrity of the chromosomes (76). Subsequent to denaturation, hybridization at 37°C allows the probe to anneal to target DNA, although several hours are required for optimal binding specificity, as outlined in the following protocol:

Initially, slides are placed in a RNase A (0.1 mg/mL) solution at 37 °C for 10 minutes, followed by a PBS wash. Then, placed in 4% PFA in PBS for 10 minutes at room temperature, washed in PBS, and then dehydrated in an ethanol series of 70%, 85%, and 100% for two minutes each in an ice water bath. They were then placed in a 2XSSC 70% formamide solution at 80°C for 2 minutes, followed by the same ethanol wash followed by the preparation of a probe solution consisting of 60% of formamide, 20 mM of Tris-HCl, 200 nM of TelC-Cy3 (Cy3-O-CCCTAACCCCTAACCCCTAA) and 200 nM of CENPB Box-FAM (FAM-O-ATTCGTTGGAAACGGGA). The solution is denatured at 85°C for 5 minutes, cooled down to 37°C, and 30 µL is added to each slide. After overnight hybridization at 37°C, slides are washed in a 2XSSC 70% formamide solution for 15 minutes at 37°C, followed by 5 minutes in PN buffer at room temperature. Finally, a counter stain with Prolong Gold Antifade with 4',6-diamidino-2-phenylindole (DAPI) is applied.

The modified PNA FISH protocol used in these experiments allow PNA probes to bind to centromeric and telomeric regions without denaturation and a shorter hybridization period:

Slides are placed into 4% PFA in PBS for ten minutes at room temperature then washed in PBS. Slides are then placed in a RNase A (0.1 mg/mL) solution at 37°C for 15 minutes, followed by a PBS wash, then treated a with pepsin (1%) in 100 mM HCl solution at

37°C for ten minutes. The slides are washed with fresh PBS and then placed in an ethanol series of 70%, 90%, and 100% for two minutes each. The probe solution used for staining was prepared and consisted of 200 nM of TelC-Cy3, (Cy3-O-TTAGGGTTAGGGTTAGGG), 200 nM of CENPB Box-FAM, (FAM-O-ATTCGTT GGAAACGGGA), 60% formamide, 1M Tris-HCl, and pure water. Approximately 15 µL of the probe solution is added to the slides and secured with a coverslip and allowed to hybridize at room temperature anywhere between 6-18 hours. After hybridization, slides are placed in PN buffer at 37°C for 10 minutes, followed by a five minute wash with PBS at room temperature. A counter stain is applied with Prolong Gold Antifade with 4',6-diamidino-2-phenylindole (DAPI). Analysis of the modified PNA FISH signal strength of TelC-Cy3 and CENPB Box-FAM probes, via fluorescence microscopy, without denaturing and in a formamide probe solution was rated after hybridization at varying times at room temperature as shown in Table 5.

TABLE 5
Signal strength over time

Probes	Time in Room Temperature		
	1 Hour	4 Hours	18 Hours
TelC	Strong	Strong	Strong
CENP B Box	Absent	Poor	Strong

The signal strength for the centromere probe, CENPB Box, required a full 18-hour hybridization period for adequate signal strength, whereas the telomere probe signal was not time-dependent. In addition, when comparing the signal strength of the telomere and centromere probes after an 18-hour hybridization period at varying temperatures between the traditional FISH and modified PNA FISH protocols, the telomere signal remains strong at all temperatures for both protocols, however, centromere signals are strongest at room temperature and at 37°C as shown in Table 6.

TABLE 6
Signal strength over varying temperatures

Probes	Modified PNA FISH			FISH
	4 °C	RT	37°C	
TelC	Strong	Strong	Strong	Strong
CENP B Box	Fair	Strong	Strong	Strong

The optimal strength of differing probe signals may vary over time and temperature, however, hybridization without denaturation remains sufficient which suggests another binding mechanism other than a PNA-DNA interaction. Therefore, without denaturation, the assay becomes more efficient, due to the ease and rapidity of its usage, as well as providing a less invasive technique that limits DNA alterations for a more reliable cytogenetic analysis.